CELL TO DENDRITE TRANSITION IN TIN BASE ALLOYS[1]

T. S. PLASKETT[2] AND W. C. WINEGARD[3]

ABSTRACT

The transition from cellular growth to dendritic growth was investigated for dilute binary alloys of zone-refined tin with lead, bismuth, and antimony in terms of the rate of growth R, the temperature gradient in the liquid ahead of the solid–liquid interface G, and the solute concentration C_0. It was found that a previous relationship describing the transition for lead base alloys applied, at least to a first approximation, for the low solute concentration tin results. At the high concentrations of solute, however, it was necessary to introduce another variable, namely the cell size at transition d_t. The transition relationships only applied for alloy systems with a distribution coefficient k_0, less than unity. For systems with $k_0 > 1$ (antimony in tin) a $k_0 < 1$ was used which was equivalent to the $k_0 > 1$. A method is described for determining this "equivalent k_0".

INTRODUCTION

Rutter and Chalmers (1953) have shown that when an alloy solidifies under certain growth conditions, the liquid adjacent to the advancing interface is constitutionally supercooled. The degree of constitutional supercooling, as shown theoretically by Tiller *et al.* (1953), is dependent upon the following variables: the rate of growth R, the temperature gradient in the liquid ahead of a solid–liquid interface G, and the solute concentration C_0. Rutter and Chalmers also showed that the cellular growth structure results from a small amount of constitutional supercooling, while Winegard and Chalmers (1954) postulated that dendritic growth would occur at larger amounts of supercooling. This was verified experimentally by Morris *et al.* (1955).

The transition from cellular to a dendritic growth mechanism was investigated by Tiller and Rutter (1956) for lead–tin alloys in terms of the growth variables. It was found that the important parameters describing the transition were C_0, $G/R^{\frac{1}{2}}$, and the orientation of the crystal. For a given concentration, the transition occurred over a range of $G/R^{\frac{1}{2}}$ values, depending upon the orientation of the crystal. The limits of the transition range, referred to as "upper" and "lower" breakdown, were linear when plotted as C_0 versus $G/R^{\frac{1}{2}}$. The exact orientation effect was not determined except that the upper breakdown was the dendrite direction.

Holmes *et al.* (1957) conducted similar experiments with silver in zone-refined lead. When these results were compared to those of Tiller and Rutter, it was found that the two systems could be related by expressing the concentration as C_0/k_0, i.e., transition occurred at the same $G/R^{\frac{1}{2}}$ ratio for the same C_0/k_0 concentration. Tiller (1956) suggested a similar relationship and expressed it as

$$G/R^{\frac{1}{2}} = A_\theta C_0/k_0 \tag{1}$$

[1]Manuscript received in original form December 14, 1959, and, as revised, May 25, 1960.
Contribution from the Department of Metallurgical Engineering, University of Toronto, Toronto 5, Canada.

[2]Present address: Department of Mines and Technical Surveys, Physical Metallurgy Division, Ottawa, Canada.
[3]Associate Professor of Metallurgy, University of Toronto.

where A_θ was a constant dependent upon the orientation. The constant A_θ was postulated to be a function of cell size since cell size was dependent upon the orientation. If

$$A_\theta = A'd_\theta \tag{2}$$

where d_θ is the cell size for a given orientation, then the general relationship becomes

$$G/R^{\frac{1}{2}} = A'd_\theta C_0/k_0. \tag{3}$$

This relationship was not verified experimentally, since cell data was not available for lead base alloys.

The primary purpose of this investigation was to determine if the more general equation (equation (1)) applied to another alloy system with a solvent material of an entirely different crystal structure than lead, namely tin, which is interlacing body center tetragonal.

EXPERIMENTAL PROCEDURE

Three tin alloys were chosen, lead in tin, bismuth in tin, and antimony in tin; the distribution coefficients for each alloy are listed in Table I. Antimony is of particular interest since it has a distribution coefficient greater than unity.

TABLE I

Alloying element in tin	Distribution coefficient, k_0
Pb	0.1
Bi	0.2
Sb	3

The alloys were prepared from zone-refined tin and chemically pure lead, bismuth, or antimony. The melting of the specimens prior to growth was done in vacuum, but growth was carried out under an atmosphere of argon. All the alloys were not analyzed, since it was shown from preliminary experiments that the percentage by weight added agreed with the analyzed value.

The solidification structures were observed on solid–liquid interfaces. The interfaces were obtained by the use of a modified Elbaum and Chalmers (1955) apparatus, which is essentially a mechanism for decanting away the liquid from the solid during solidification. The apparatus, which is a two-part graphite boat in a larger graphite container, is shown in Fig. 1(*a*) before decanting, and 1(*b*) after decanting. Solidification began from the water-cooled copper block placed in the end of the movable portion of the graphite boat; this is shown on the right side of Fig. 1(*b*). Freezing was allowed to proceed from right to left until the interface reached the stationary half of the boat. The movable half was then accelerated to the right along the track of the larger graphite container; the solid was thus pulled away from the liquid to expose the solid–liquid interface.

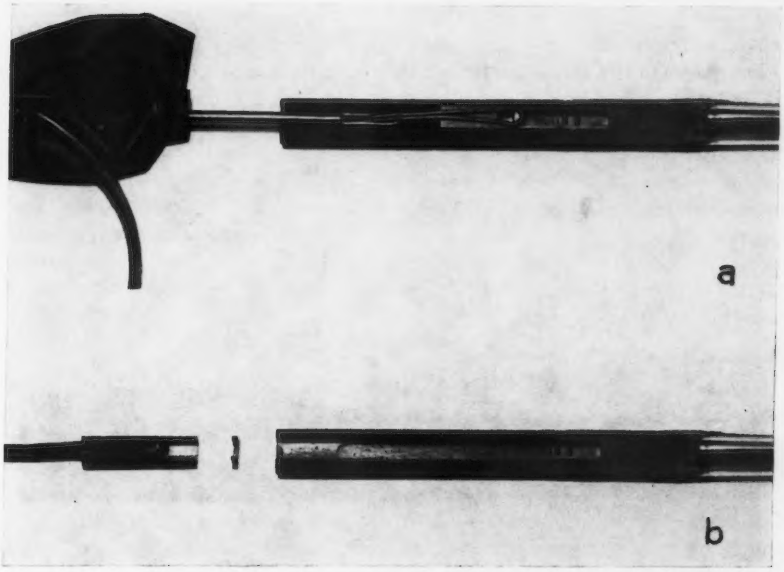

FIG. 1. Detail view of the graphite boat for growing the specimen and for decanting away the liquid (*a*) before decanting, (*b*) after decanting.

It is important when using this technique to maintain unidirectional heat flow, and two special features were used to ensure that this would be the case. Firstly, the two-part inner boat was surrounded by a graphite case, and the air gap between them helped to prevent lateral heat loss. Secondly, a small graphite insert, seen in Fig. 1(*b*), between the movable and stationary halves of the boat, prevented heat being transferred along the graphite boat faster than through the solidifying metal.

The growth conditions were measured in a manner similar to that used by Tiller and Rutter, except that only two thermocouples were used, and these were placed directly in the melt 1 cm apart. The position of the thermocouples, which were inside the horizontal alundum tubes, is shown in Fig. 1. The liquid was decanted when the solid had advanced to the first thermocouple. Since the thermocouples were connected as a differential, a reading at this point gave the temperature gradient in the liquid directly.

The growth conditions were varied by changing the longitudinal temperature gradient in a tube furnace that surrounded the boat, and by varying the rate at which this gradient was moved along the specimen. This provided a range of G values from 1.5 to 13.0° C/cm and R values from 0.001 to 0.015 cm/sec; this range is larger than that obtained using the thermal valve technique of Tiller and Rutter.

OBSERVATIONS AND RESULTS

Interface Structures

The stages in the transition from a cellular interface to a dendritic interface are shown in a series of photomicrographs in Fig. 2. This series was taken from a 0.2 at.% lead in tin alloy, but is typical for all concentrations and for the other tin alloys investigated. Figure 2(*a*) is the solid–liquid interface of a specimen grown under the highest $G/R^{\frac{1}{2}}$ ratio. Each successive photomicrograph represents an interface of a specimen grown at lower $G/R^{\frac{1}{2}}$ ratios. The transition from cells to dendrites was defined as that point when the cell walls became branched or disappeared. This is shown in Fig. 2(*d*) for this particular series. This criterion is similar to that used by Tiller and Rutter, and Holmes *et al.*

Growth Conditions for Transition

The growth conditions for the transition are shown graphically for the three tin alloys in Figs. 3, 4, and 5, where the results are plotted as C_0/k_0 versus $G/R^{\frac{1}{2}}$. The value of k_0 used for the antimony in tin system is not 3 but 0.6, which is defined as k_0', the equivalent k_0 value. The reason for using this value and the method for determining the equivalent k_0 is discussed later. The curves shown in the above figures represent the growth conditions for transition; to the right of the curves are the growth conditions for cells, and to the left are those for dendrites. The transition curves are not linear, and there is no apparent range of $G/R^{\frac{1}{2}}$ ratios over which transition occurs for a given solute concentration.

Orientation of Crystals Observed on the Interfaces

Each specimen examined was polycrystalline with the crystal size dependent upon the concentration. At low concentrations, the crystal size was very large and the orientation of each individual crystal could be determined. A random sample of the crystals showed that the orientations were within 20° of the reported dendrite direction [110]. At the higher concentrations, the crystal size was too small to determine the orientation of each crystal and too large for a conclusive determination of the preferred orientation. Sufficient evidence was obtained, however, to indicate that some type of preferred orientation existed. The structures observed on a polycrystalline interface were similar on all the crystals, thus indicating that the solidification structures in tin were not sensitive to small changes in orientation.

Cell Size

It was observed for all three alloy systems that the cell size of crystals grown in the cellular region decreased as $G/R^{\frac{1}{2}}$ decreased. The cell size measurements, an average of five readings, are tabulated in Table II along with the corresponding growth conditions. A scatter diagram showing the decrease in cell size as $G/R^{\frac{1}{2}}$ decreased for lead in tin alloys is plotted in Fig. 6; the results of the other alloy systems give similar diagrams. It is also evident from the scatter diagrams that, within the concentration range investigated, the cell

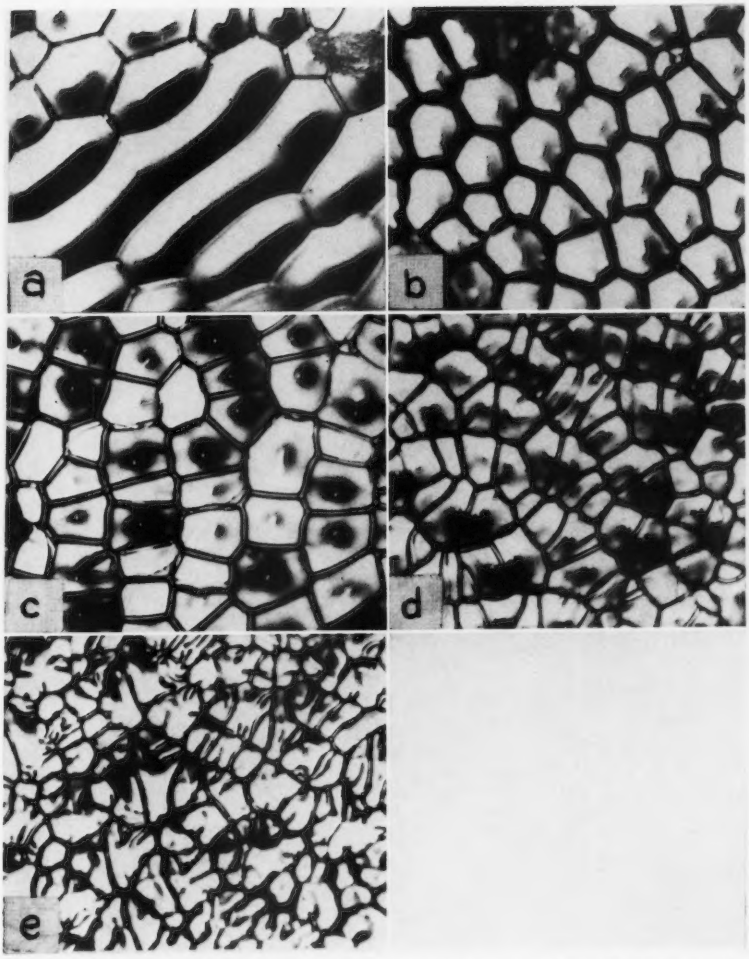

FIG. 2 Transition from a cellular to dendritic interface for a 0.2 at.% Pb in Sn alloy (150×). Growth condition for each structure is: (*a*) $G/R^{\frac{1}{2}} = 430$; (*b*) $G/R^{\frac{1}{2}} = 356$; (*c*) $G/R^{\frac{1}{2}} = 200$; (*d*) $G/R^{\frac{1}{2}} = 64$; (*e*) $G/R^{\frac{1}{2}} = 31$.

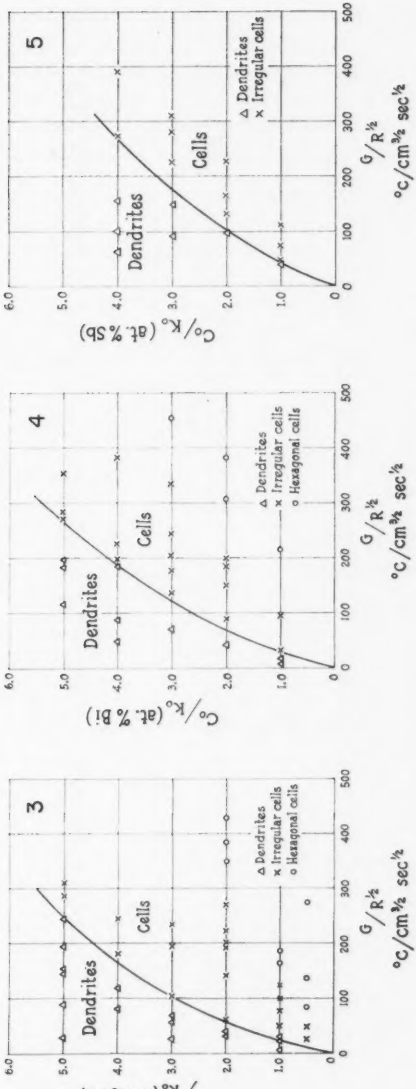

FIG. 3. Growth conditions for the cell to dendrite transition, Pb in Sn.
FIG. 4. Growth conditions for the cell to dendrite transition, Bi in Sn.
FIG. 5. Growth conditions for the cell to dendrite transition, Sb in Sn. The equivalent k_0 value is used.

TABLE II

Alloy element in tin	C_0, at.%	G, °C/cm	R, cm/sec	$G/R^{\frac{1}{2}}$, °C/cm$^{3/2}$ sec$^{1/2}$	Cell size d, cm
Pb	.50	10.25	.0011	310	.00590
		10.00	.0012	285	.00614
	.40	13.50	.0030	245	.00515
		10.25	.0033	180	.00520
		9.00	.0030	164	.00600
	.30	10.75	.0021	234	.00530
		8.00	.0017	195	.00560
		7.25	.0051	102	.00548
	.20	9.50	.0005	430	.00820
		11.75	.0011	356	.00553
		11.25	.0017	274	.00492
		11.00	.0017	269	.00600
		10.25	.0021	223	.00525
		7.00	.0012	200	.00686
		10.25	.0028	193	.00520
		10.00	.0051	141	.00522
		7.00	.0119	64	.00500
	.10	9.25	.0025	185	.00615
		8.75	.0028	165	.00588
		8.75	.0051	123	.00480
		7.50	.0055	101	.00520
		8.00	.0062	101	.00475
		6.50	.0068	79	.00425
		6.25	.0152	51	.00360
		4.25	.0254	27	.00327
	.05	8.50	.0038	136	.00587
		7.50	.0076	86	.00446
		6.00	.0152	49	.00408
		4.25	.0237	28	.00304
Bi	1.00	10.00	.0008	357	.00558
		8.00	.0019	281	.00580
		9.75	.0013	271	.00604
		8.75	.0020	194	.00632
	.80	10.00	.0007	385	.00608
		9.25	.0017	226	.00610
		8.75	.0019	199	.00521
		9.00	.0024	184	.00615
	.60	10.00	.0050	455	.00827
		10.75	.0010	336	.00535
		8.75	.0013	243	.00617
		10.00	.0023	208	.00497
		9.50	.0028	179	.00545
		9.00	.0042	138	.00485
		5.75	.0068	70	.00449
	.40	9.75	.0010	305	.00790
		9.00	.0021	184	.00493
		10.50	.0048	152	.00466
		7.50	.0068	91	.00342
		6.25	.0207	43	.00290
	.20	10.00	.0021	217	.00503
		7.50	.0059	97	.00426
		5.25	.0237	34	.00292
		3.25	.0402	16	.00235
Sb	2.4	12.50	.0010	391	.00617
		10.00	.0014	270	.00585
	1.8	11.00	.0012	314	.00531
		10.50	.0014	284	.00576
		9.25	.0017	226	.00628
	1.2	11.50	.0025	230	.00452
		9.75	.0036	163	.00498
		9.25	.0038	149	.00482
	.6	8.75	.0059	114	.00485
		7.50	.0102	74	.00372
		7.00	.0203	49	.00365

size is independent of the solute concentration. The best curves drawn through the points for each alloy are shown in Fig. 7; these indicate that the cell size is also independent of the solute addition.

Since the $G/R^{\frac{1}{2}}$ ratio for transition is dependent upon the concentration (see Figs. 3, 4, and 5), it would be expected therefore that the cell size at the transition point, defined as d_t, should vary with concentration. This variation, as shown in Fig. 8 for the three tin alloys, is linear. In order to keep the curves on the same scale, the concentration was expressed as C_0/k_0 and the k_0 value used for antimony in tin was again the equivalent k_0 of 0.6.

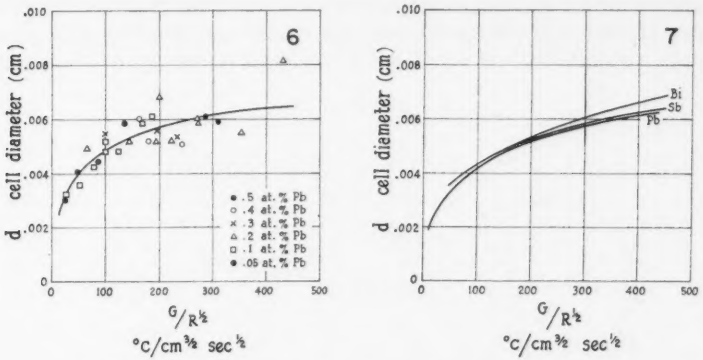

FIG. 6. Scatter diagram of cell size versus the parameter $G/R^{\frac{1}{2}}$, Pb in Sn.
FIG. 7. Cell size versus $G/R^{\frac{1}{2}}$ for all three tin alloys.

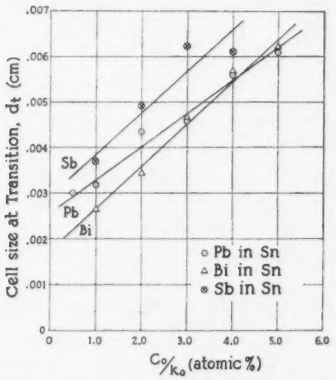

FIG. 8. Cell size at the cell to dendrite transition for all three alloys. The equivalent k_0 value is used for the Sb in Sn alloy.

Summary of Observations and Results

(1) The transition from cells to dendrites when plotted as $G/R^{\frac{1}{2}}$ versus C_0/k_0 was not linear.

(2) Transition did not occur, for a given concentration, over a range of $G/R^{\frac{1}{2}}$ ratios.

(3) For cellular growth, the cell size was independent of solute concentration and solute type, but dependent only upon G and R.

(4) The cell size at transition from cells to dendrites varied linearly with the solute concentration.

DISCUSSION

Comparison of Lead and Tin Base Alloys

The results of the lead base alloys and the tin base alloys are compared in Fig. 9. The lead base alloys are taken directly from the paper by Holmes *et al.*, and the main differences between the two systems are:

(*a*) The transition was not found to occur over a range of $G/R^{\frac{1}{2}}$ ratios for a given concentration. From the crystal orientation measurements, it appears that at least within 20° of the dendrite direction there is no orientation effect.

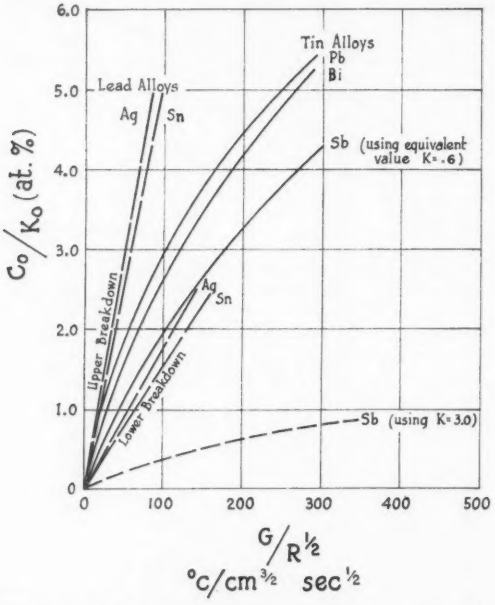

FIG. 9. Comparison of the cell to dendrite transition curves for the tin and lead alloys. (Lead alloy curves taken from Holmes *et al.* (1957).)

(*b*) The relationship between C_0/k_0 and $G/R^{\frac{1}{2}}$ for transition is not linear for the tin alloys; this is in contrast to the results for the lead alloys. The difference may in part be due to the fact that the present investigation was carried to higher C_0/k_0 ratios. Holmes *et al.*, when comparing the two lead alloys, extrapolated to a C_0/k_0 value of 5, while the actual experimental values only went to 3.5 for tin in lead and 2.4 for silver in lead. The tin results may also be considered as being linear if taken only to the same value.

Since the curves, as shown in Fig. 9, are so close together, it seems that there is no major effect of solvent crystallography and that the onset of dendritic growth can be predicted from equation (1) at least for low concentrations. When the entire concentration range is included, however, the equation does not apply. This suggests that one of the parameters is not correct or that another variable influences the transition.

Cell Size at Transition

As previously shown, the cell size at transition decreases as the concentration decreases. This variation can be explained in terms of the cell profile and provides further insight into the mechanism of the cell to dendrite transition. Consider the schematic diagram in Fig. 10. The diagram represents pairs of alloys grown at various $G/R^{\frac{1}{2}}$ values. The concentration within each

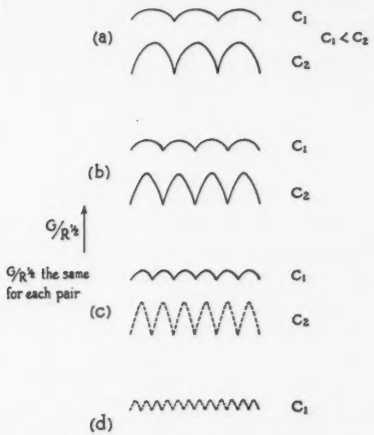

FIG. 10. Effect of varying the value of $G/R^{\frac{1}{2}}$ on the cell profile for two different concentrations.

pair is C_1 and C_2, respectively, where $C_2 > C_1$ and the $G/R^{\frac{1}{2}}$ for both concentrations in a pair is the same. The cell size of each pair is the same since it was observed that, within the cellular range, cell size was independent of composition and dependent only upon $G/R^{\frac{1}{2}}$. The diagram shows this decrease in cell size as $G/R^{\frac{1}{2}}$ is lowered.

As $G/R^{\frac{1}{2}}$ is lowered, it may be assumed that the amount of constitutional supercooling ahead of the interface tends to increase. The increase in supercooling can be reduced if solute is taken away from the tip of the advancing interface and placed in the cell wall. This will lead to an increase in the cell wall area (a decrease in cell size) as $G/R^{\frac{1}{2}}$ decreases. The alloy of concentration C_2, however, has more solute to accommodate, and yet has the same cell size as the alloy of composition C_1. The extra solute can be accounted for if the cusps in the high concentration alloy are deeper than in the low concentration alloy. Again, this is shown in Fig. 10. Depending on the depth of the cusps

and on the cell diameter, the cell profile will tend towards a triangular shape in two dimensions or a pyramidal shape in three dimensions, pyramidal instead of conical due to the platelet system (Rosenberg and Tiller 1957). Once the cell profile reaches the pyramidal shape, a further decrease in cell size does not increase the total volume available as a "solute sink". Solute will then build up ahead of the cellular interface, causing larger amounts of constitutional supercooling and thus dendritic growth. This occurs in Fig. 10(*c*) for the C_2 concentration alloy; any further decrease in the cell diameter does not increase the total area between the cells for this concentration, i.e., there is no increase in area between the cells shown in Fig. 10(*b*) and (*c*). This does not occur for C_1 alloy until a lower $G/R^{\frac{1}{2}}$ ratio is reached (Fig. 10(*c*)). In other words, for the C_1 case, the cells can continue to decrease and produce more "solute sinks" to accept the added solute caused by the lowering of $G/R^{\frac{1}{2}}$ since they have not reached the limiting pyramidal shape.

The above argument not only helps in the understanding of the cells to dendrite transition, but also suggests that any relationship between C_0, k_0, and $G/R^{\frac{1}{2}}$ for the breakdown should include the parameter d_t, the cell size at transition.

$$G/R^{\frac{1}{2}} = A' d_t C_0/k_0 \tag{4}$$

(where d_t is the cell size at transition) was applied to the three tin alloys using the equivalent value of k_0 for the Sn–Sb alloy.

The three curves are plotted in Fig. 11. A linear plot was obtained indicating that the cell size is an important variable in describing the transition. The above relationship cannot be tested for the lead base alloys since no cell size data at transition are available.

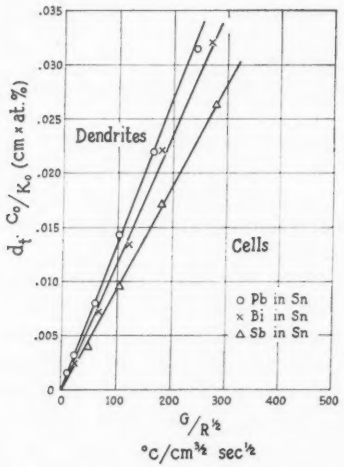

FIG. 11. Growth conditions for the cell to dendrite transition with the variable of cell diameter included.

The relationship expressed in equation (4) is similar to that developed by Tiller (1956) to account for the orientation effect observed in lead alloys. From the present work, it appears that cell size is even more important than previously thought in determining when transition occurs for any given alloy, since cell size at transition depends upon concentration.

Distribution Coefficient Greater than Unity

The antimony in tin results are plotted in Fig. 9 using a k_0 value of 3 and an equivalent k_0 value of 0.6. The equivalent k_0 value is defined as the distribution coefficient of a $k_0 < 1$ type phase diagram which will give exactly the same amount of constitutional supercooling under the same growth conditions. To find this equivalent k_0, it is first necessary to reverse the sign of the slope of the liquidus curve; next, the value of solute depletion ahead of the $k_0 > 1$ type alloy must be equated against the solute build-up for equivalent $k_0 < 1$ alloy so that the values are the same but opposite in sign. If k_0' represents the equivalent k_0, then

$$\left(\frac{C_0}{k_0'} - C_0\right) = -\left(\frac{C_0}{k_0} - C_0\right)$$

$$k_0' = \frac{k_0}{2k_0 - 1}.$$

The expression used for the solute build-up and depletion are those developed by Tiller *et al.* (1953) from the work on the redistribution of solute ahead of plane interface, assuming the same non-equilibrium conditions.

The equivalent k_0 value for antimony in tin is 0.6. When the actual k_0 value is used, as shown in Fig. 9 by the dotted line, the results are not in agreement but they are when the equivalent value is used. This is because the equivalent k_0 must be used whenever the value of C_0/k_0 is used as an indication of the freezing point depression such as is used in the constitutional supercooling argument. The use of an equivalent k_0 makes all concentration readings positive with respect to the original concentration.

CONCLUSIONS

It can be concluded that the cell to dendrite transition in the tin base alloys is dependent, as was found for the lead base alloys, on the growth variables. This again indicates that the important concept in this transition is constitutional supercooling. It can also be concluded that the general relationship describing the transition is not markedly affected by the solvent crystallography. Although the relationship describing this transition still does not have a complete theoretical basis, this investigation, however, does point out the importance of cell size on the transition and the effect of a distribution coefficient greater than unity.

ACKNOWLEDGMENTS

The authors are grateful to the University of Toronto and the Defence Research Board of Canada (Grant 9535-01) for financial support.

REFERENCES

ELBAUM, C. and CHALMERS, B. 1955. Can. J. Phys. **33**, 196.
HOLMES, E. L., RUTTER, J. W., and WINEGARD, W. C. 1957. Can. J. Phys. **35**, 1223.
MORRIS, W., TILLER, W. A., RUTTER, J. W., and WINEGARD, W. C. 1955. Trans. Am. Soc. Metals, **47**, 463.
ROSENBERG, A. and TILLER, W. A. 1957. Acta Met. **5**, 565.
RUTTER, J. W. and CHALMERS, B. 1953. Can. J. Phys. **31**, 15.
TILLER, W. A. 1956. Can. J. Phys. **34**, 729.
TILLER, W. A., JACKSON, K. A., RUTTER, J. W., and CHALMERS, B. 1953. Acta Met. **1**, 428.
TILLER, W. A. and RUTTER, J. W. 1956. Can. J. Phys. **34**, 96.
WINEGARD, W. C. and CHALMERS, B. 1954. Trans. Am. Soc. Metals, **46**, 1214.

A THEORY OF IONOSPHERIC CURRENTS ASSOCIATED WITH AURORAE. I[1]

J. T. WEAVER[2] AND R. SKINNER

ABSTRACT

The current distributions induced by dynamo action in a sheet of partially ionized gas moving with uniform velocity across a perpendicular magnetic field are derived for the case when the gas contains an elliptical region of greater ionization density. Special attention is paid to processes occurring away from the ends of a long narrow ellipse in which the ionization density is much greater than the surrounding region.

The results are discussed in relationship to conditions pertaining in the ionosphere when a long homogeneous auroral arc is present. It is concluded that a line current, whose magnitude is linearly dependent on the height-integrated Cowling conductivity within the arc, flows along the arc.

1. INTRODUCTION

One of the first observed characteristics of auroral displays was their close relationship with geomagnetic storms. Although extensive analyses of geomagnetic disturbances have been conducted on a statistical and world-wide basis, surprisingly little attention has been paid to the magnetic disturbances associated with individual auroral displays.

In recent years, it has been realized that Chapman's S_D current systems deduced from statistical studies, while providing much valuable information, do not describe the actual ionospheric currents flowing at any particular time. In particular, Meek (1955) found from his study of ionospheric, auroral, and magnetic variations that Chapman's average current systems were inconsistent with the individual magnetic disturbances occurring at Saskatoon at any particular time. Therefore, it seems preferable to examine individual magnetic disturbances rather than long-term averages in order to obtain a clearer understanding of the cause of magnetic variations and, in particular, their relationship with auroral displays.

In this paper, we examine the problem from a theoretical point of view. We shall accept the hypothesis that dynamo action on an ionospheric region of increased ionization density (assumed coincident with an auroral display) is the physical mechanism responsible for induced ionospheric currents, and hence those magnetic disturbances associated with the auroral display. With this as a basis, the subsequent work is devoted to a mathematical investigation of the nature of the current systems associated with certain types of aurorae. The current system in a thin sheet of partially ionized gas containing an elliptical region of greater ionization density is calculated. The solutions to this problem are then adapted for application to the ionosphere so that the current flows associated with a long homogeneous auroral arc can be found.

[1]Manuscript received May 2, 1960.
Contribution from the Physics Department, University of Saskatchewan, Saskatoon, Saskatchewan.
[2]Now at the Department of Mathematics, University of Saskatchewan.

2. THE CONDUCTIVITIES OF A PARTIALLY IONIZED GAS

The conductivity of an ionized gas in the presence of a magnetic field is anisotropic. In the direction of the magnetic field there is a longitudinal conductivity $\sigma_\parallel$, in the direction of the electric field a Pedersen conductivity σ_1, and perpendicular to both fields a Hall conductivity σ_2. Thus the current density vector $\mathbf{j}$ can be written as

$$\mathbf{j} = \sigma_\parallel \mathbf{E}'_\parallel + \sigma_1 \mathbf{E}'_\perp + \sigma_2 \mathbf{h} \times \mathbf{E}' \tag{1}$$

where $\mathbf{h} = \mathbf{H}/H$ is a unit vector in the direction of the magnetic field. $\mathbf{E}'_\parallel$ and $\mathbf{E}'_\perp$ denote the respective components of the electric field $\mathbf{E}'$ in the direction of, and perpendicular to the magnetic field.

The anisotropy of the conductivity of the ionosphere, which can be considered as a lightly ionized gas, was pointed out by Pedersen (1927) and Cowling (1933), who calculated expressions for σ_1 and σ_2 respectively. A detailed examination of the possible effect of the different conductivities on induced dynamo currents in the ionosphere was undertaken by Martyn (1948) and Baker and Martyn (1953) in an attempt to account for observed discrepancies between the magnitude of the S_q field predicted by the dynamo theory and the observed S_q magnetic variations.

The conductivities $\sigma_\parallel$, σ_1, and σ_2 for a lightly ionized gas containing electrons, positive ions (carrying a positive electronic charge), and neutral particles can be derived most simply using mean-free-path theory. Cowling (1945) showed that for the conditions found in the ionosphere this gives approximately the same expressions as the accurate theory. It is assumed that the density of electrons n equals the density of the positive ions, but is small compared with the density of the neutral particles, and also that the positive ions and neutral particles have equal masses. It can then be shown that (Dungey 1958)

$$\sigma_\parallel = ne^2\left(\frac{1}{m_e\nu_e} + \frac{1}{m_i\nu_i}\right) \tag{2}$$

$$\sigma_1 = ne^2\left[\frac{\nu_e}{m_e(\nu_e^2+\omega_e^2)} + \frac{\nu_i}{m_i(\nu_i^2+\omega_i^2)}\right] \tag{3}$$

$$\sigma_2 = ne^2\left[\frac{\omega_e}{m_e(\nu_e^2+\omega_e^2)} - \frac{\omega_i}{m_i(\nu_i^2+\omega_i^2)}\right] \tag{4}$$

where $-e$ is the electronic charge, m_e and m_i are respectively the masses of an electron and a positive ion, and ν_e and ν_i are their respective collisional frequencies with neutral particles. In the usual notation ω_e and ω_i represent the gyrofrequencies of the electrons and ions respectively defined by the relation

$$\omega_{e,i} = eH/m_{e,i}. \tag{5}$$

It has been found that the combination $(\sigma_1^2+\sigma_2^2)/\sigma_1$ plays an important role in ionospheric electrodynamic equations. Chapman calls this expression the Cowling conductivity. Denoting it by σ_3 we have

$$\sigma_3 = \frac{\sigma_1^2+\sigma_2^2}{\sigma_1} = \frac{ne^2}{\nu_e\nu_i+\omega_e\omega_i}\left(\frac{\nu_i}{m_e}+\frac{\nu_e}{m_i}\right). \tag{6}$$

3. CURRENT FLOW IN A SHEET OF LIGHTLY IONIZED GAS

We shall calculate the current system in a thin sheet of lightly ionized gas containing an elliptical, anomalous patch of greater ionization density. The gas is considered to be moving with a uniform velocity perpendicular to a constant magnetic field. As such the problem is somewhat artificial in nature, the physical conditions being idealized for mathematical convenience.

Consider a horizontal plane sheet of the partially ionized gas having perfectly insulating regions above and below it. We assume that all vertical currents are prevented in the sheet by a vertical polarization field set up by the accumulation of charge on the upper and lower surfaces of the sheet. Thus, if a right-handed set of axes are defined such that the x and y axes are in the plane of the sheet and the z-axis is vertically upwards the current density vector $\mathbf{j}$ has components $(j_x, j_y, 0)$ and the equation of continuity can be written in the form

$$\frac{\partial j_x}{\partial x}+\frac{\partial j_y}{\partial y} = 0, \tag{7}$$

provided that no sources or sinks of charges exist in the sheet. This equation will be satisfied if we introduce a current function $J(x,y)$ defined by the relations

$$j_x = \partial J/\partial y, \tag{8}$$

$$j_y = -\partial J/\partial x. \tag{9}$$

Let the magnetic field $\mathbf{H}$ be directed vertically downwards perpendicular to the sheet. Thus in (1) $\mathbf{h} = -\mathbf{k}$, where $\mathbf{k}$ is a unit vector in the z direction and (1) reduces to

$$\mathbf{j} = \underset{\sim}{\Sigma}.\mathbf{E}' \tag{10}$$

where

$$\underset{\sim}{\Sigma} = \begin{pmatrix} \sigma_1 & \sigma_2 \\ -\sigma_2 & \sigma_1 \end{pmatrix} \tag{11}$$

is a matrix quantity representing the generalized anisotropic conductivity.

If the ionized gas has a uniform mass-velocity $\mathbf{v}$ there will be an induced dynamo field $\mathbf{E} = \mathbf{v}\times\mathbf{H}$ experienced by the gas. If, furthermore, there is an ionization anomaly in the gas, charge accumulations will be set up on the boundaries due to the fact that currents can flow more readily within the anomalous region of high conductivity than they can in the surrounding medium. The charge accumulation will increase until it has created an electrostatic polarization field which is just sufficient to retard the current flow within the anomaly to such an extent that the rate of arrival of charge at the boundary is balanced by the rate at which charge can leak away in the surrounding gas. Thus the total electric field $\mathbf{E}'$ can be written

$$\mathbf{E}' = \mathbf{E}-\text{grad}\, S \tag{12}$$

where S is the potential of the polarization field.

After substituting for $\mathbf{E}'$ in (10) and introducing J defined by (8), (9) we have

$$\partial J/\partial y = -\sigma_1 \partial V/\partial x - \sigma_2 \partial V/\partial y \tag{13}$$

$$\partial J/\partial x = -\sigma_2 \partial V/\partial x + \sigma_1 \partial V/\partial y \tag{14}$$

where

$$V = S + H(xv_y - yv_x). \tag{15}$$

Elimination of V from these equations gives

$$\nabla^2 J = 0 \tag{16}$$

where ∇^2 is the Laplacian operator in two dimensions. Similarly, elimination of J yields

$$\nabla^2 V = 0 \tag{17}$$

except at points on the boundary of the anomaly, where the net charge density is no longer zero. Hence by (15), we have also

$$\nabla^2 S = 0 \tag{18}$$

except on the boundary.

The solutions of (18) will be derived for the case when the gas contains an elliptical region of greater ionization density. Let the potential of the polarization field set up by the accumulation of charge on the elliptical boundary be denoted by S inside the ellipse and S' outside. Clearly S and S' must satisfy the following conditions:

(i) $\nabla^2 S = 0$ within the ellipse,
(ii) $\nabla^2 S' = 0$ outside the ellipse,
(iii) $S = S'$ on the boundary of the ellipse,
(iv) S is finite inside the ellipse,
(v) $S' \to 0$ as the distance from the ellipse approaches infinity,
(vi) the normal component of $\mathbf{j}$ is continuous on the boundary of the ellipse.

Let the equation of the ellipse be

$$\frac{x^2}{a^2} + \frac{y^2}{b^2} = 1 \tag{19}$$

in the complex t-plane, where

$$t = x + iy. \tag{20}$$

Consider the conformal transformation to the ζ-plane given by

$$\zeta = \text{arc cosh } (t/p) \tag{21}$$

where

$$p = \sqrt{(a^2 - b^2)}. \tag{22}$$

If we denote the co-ordinates in the ζ-plane by (ξ, η),

$$\zeta = \xi + i\eta, \tag{23}$$

the interior of the ellipse with a cut taken along the real axis from $z = -a$ to $z = p$ is transformed into the region $0 \leqslant \xi < \xi_0$, $-\pi \leqslant \eta \leqslant \pi$, where

$$\xi_0 = \text{arc tanh } (b/a). \tag{24}$$

The elliptical contour is transformed into the line $\xi = \xi_0$ while the remainder of the contour representing the real axis cut in the t-plane is transformed into the lines $\eta = \pm\pi (0 \leqslant \xi \leqslant \xi_0)$, $\xi = 0 (-\pi \leqslant \eta \leqslant \pi)$ in the ζ-plane. The exterior of the ellipse corresponds to the region $\xi > \xi_0$, $-\pi \leqslant \eta \leqslant \pi$. Figure 1 illustrates the transformation.

Solutions for S and S' satisfying the conditions (i) to (v) are

$$S_\omega = \sum_\omega \{2A \cosh \omega\xi \cos \omega\eta - 2B \sinh \omega\xi \sin \omega\eta\} \tag{25}$$

$$S'_\omega = \sum_\omega \{A(1+e^{2\omega\xi_0}) \cos \omega\eta + B(1-e^{2\omega\xi_0}) \sin \omega\eta\} e^{-\omega\xi} \tag{26}$$

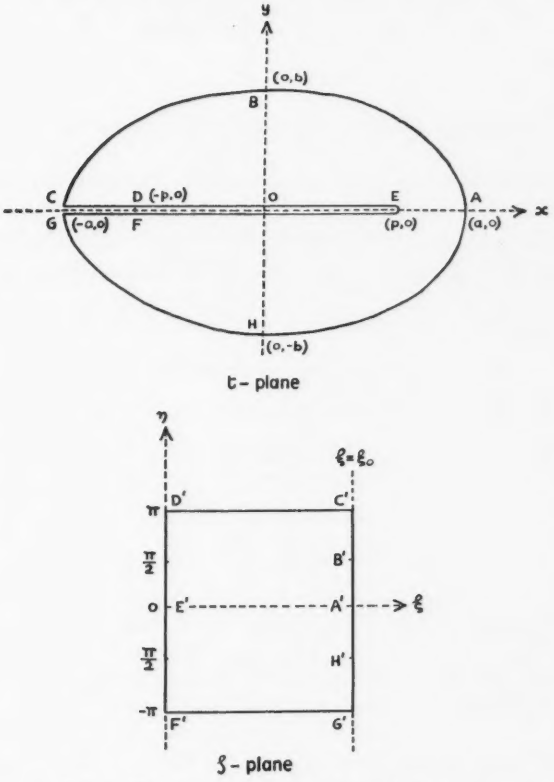

FIG. 1. The transformation $\zeta = \text{arc cosh } (t/p)$.

where $A = A(\omega)$ and $B = B(\omega)$ are constants. A and B can be evaluated by means of the boundary condition (vi). This requires that j_ξ be continuous at $\xi = \xi_0$. Now in the ζ-plane

$$j_\xi = -\sigma_1 \partial V/\partial\xi - \sigma_2 \partial V/\partial\eta \; ; \tag{27}$$

thus we require

$$\sigma_1 \left.\frac{\partial V}{\partial \xi}\right|_{\xi_0} + \sigma_2 \left.\frac{\partial V}{\partial \xi}\right|_{\xi_0} = \sigma_1' \left.\frac{\partial V'}{\partial \xi}\right|_{\xi_0} + \sigma_2' \left.\frac{\partial V'}{\partial \eta}\right|_{\xi_0} \tag{28}$$

where dashed quantities refer to the region outside the ellipse. Substitution of the partial derivatives of V and V' in this equation yields, after some lengthy algebraic manipulation, the following expressions for A and B:

when $\omega \neq 1$,

$$A = B = 0 \; ; \tag{29}$$

when $\omega = 1$,

$$A = \tfrac{1}{2} pE\alpha, \qquad B = \tfrac{1}{2} pE\beta \tag{30}$$

where

$$\alpha = \frac{b}{\Delta}\left[(a+b)\sigma_1'(\sigma_2-\sigma_2') \sin\phi + \{(a\sigma_1+b\sigma_1')(\sigma_1-\sigma_1')+a(\sigma_2-\sigma_2')^2\} \cos\phi\right] \tag{31}$$

$$\beta = \frac{a}{\Delta}\left[(a+b)\sigma_1'(\sigma_2-\sigma_2') \cos\phi - \{(b\sigma_1+a\sigma_1')(\sigma_1-\sigma_1')+b(\sigma_2-\sigma_2')^2\} \sin\phi\right] \tag{32}$$

$$\Delta = (a\sigma_1+b\sigma_1')(b\sigma_1+a\sigma_1')+ab(\sigma_2-\sigma_2')^2. \tag{33}$$

The angle ϕ introduced for convenience in the above equation is the inclination of $\mathbf{E}$ with the x-axis, i.e. $E_x = E\cos\phi$, $E_y = E\sin\phi$.

Thus the general solutions for S and S' are

$$S = pE(\alpha \cosh\xi \cos\eta - \beta \sinh\xi \sin\eta) \tag{34}$$

$$S' = \tfrac{1}{2} pE[\alpha(1+e^{2\xi_0}) \cos\eta + \beta(1-e^{-2\xi_0}) \sin\eta]e^{-\xi}. \tag{35}$$

Complex potentials w and w' can be found such that $\mathrm{Rl}\, w = S$ and $\mathrm{Rl}\, w' = S'$. Transformed into the t-plane these are

$$w = E(\alpha+i\beta)t \tag{36}$$

$$w' = E(a\alpha - ib\beta)\{t - \sqrt{(t^2-p^2)}\}/(a-b). \tag{37}$$

There is a one–one correspondence between the w-plane and the t-plane. However, w' is a two-valued function since a plus or minus sign could be placed in front of the square root sign. A one–one correspondence between w' and t can be set up by replacing the t-plane by a Riemann surface of two sheets with the connecting cut from $-p$ to p.

As a special case we can let $a \to b$ so that the ellipse approaches a circle. When $a \to b$, and the axes are rotated so that $\mathbf{E}$ is in the direction of the x-axis, $p \to 0$, $\alpha \to \alpha_0$, $\beta \to \beta_0$, $w \to w_0$, and $w' \to w'_0$ where

$$w_0 = E(\alpha_0 + i\beta_0)t \tag{38}$$

$$w_0' = Ea^2(\alpha_0 - i\beta_0)t^{-1} \tag{39}$$

$$\alpha_0 = \frac{(\sigma_1^2 - \sigma_1'^2) + (\sigma_2 - \sigma_2')^2}{(\sigma_1 + \sigma_1')^2 + (\sigma_2 - \sigma_2')^2} \tag{40}$$

$$\beta_0 = \frac{2\sigma_1'(\sigma_2 - \sigma_2')}{(\sigma_1 + \sigma_1')^2 + (\sigma_2 - \sigma_2')^2}. \tag{41}$$

By putting $t = re^{i\theta}$ and taking the real parts of w_0 and w_0' we obtain expressions for S_0 and S_0' in polar co-ordinates:

$$S_0 = QEr \cos(\theta + \epsilon) \tag{42}$$

$$S_0' = QEr^{-1}a^2 \cos(\theta + \epsilon) \tag{43}$$

where

$$Q^2 = \alpha_0^2 + \beta_0^2 = \frac{(\sigma_1 - \sigma_1')^2 + (\sigma_2 - \sigma_2')^2}{(\sigma_1 + \sigma_1')^2 + (\sigma_2 - \sigma_2')^2} \tag{44}$$

and

$$\tan \epsilon = \beta_0/\alpha_0 = \frac{2\sigma_1'(\sigma_2 - \sigma_2')}{(\sigma_1^2 - \sigma_1'^2) + (\sigma_1 - \sigma_1')^2}. \tag{45}$$

These expressions agree with those derived by Martyn (1953), who discussed the induced current systems and hydrodynamic motions of a cylindrical blob of enhanced ionization in the ionosphere.

Of very special interest also is the case when $a \gg b$. The ellipse is then very elongated, and as $a \to \infty$ it approaches a strip of infinite length and breadth b. When $a \gg b$ so that terms of order $(b/a)^2$ and higher may be neglected we have $\alpha \doteqdot \alpha_1$ and $\beta \doteqdot \beta_1$, where

$$\alpha_1 = \frac{1}{\sigma_1\sigma_1'}[\sigma_1'(\sigma_2 - \sigma_2') \sin \phi + \{\sigma_1(\sigma_1 - \sigma_1') + (\sigma_2 - \sigma_2')^2\} \cos \phi]\ (b/a) \tag{46}$$

$$\beta_1 = \beta_1' + \beta_1'' \tag{47}$$

$$\beta_1' = \frac{1}{\sigma_1}[(\sigma_2 - \sigma_2') \cos \phi + (\sigma_1 - \sigma_1') \sin \phi] \tag{48}$$

$$\beta_1'' = \frac{1}{\sigma_1^2\sigma_1'}[(\sigma_2 - \sigma_2')\{\sigma_1\sigma_1' - (\sigma_1^2 + \sigma_1'^2) - (\sigma_2 - \sigma_2')^2\} \cos \phi + \sigma_1'\{\sigma_1'(\sigma_1 - \sigma_1') - (\sigma_2 - \sigma_2')^2\} \sin \phi]\ (b/a). \tag{49}$$

It will be seen that α_1 and β_1'' are of order (b/a) compared with β_1' which is of order unity. Hence α_1 is small compared with β_1 which is itself approximately equal to β_1'.

The polarization field and current distribution away from the ends of the strip can be investigated by taking $|t| \ll a$. In this case $w \doteqdot w_1$ and $w' \doteqdot w_1'$ where

$$w_1 = E(\alpha_1+i\beta_1)t \tag{50}$$

$$w_1' = \begin{cases} E[(t-ia-ib)(\alpha_1-i\beta_1'b/a)-b\beta_1'], & \text{Im } t > 0 \\ E[(t+ia+ib)(\alpha_1-i\beta_1'b/a)+b\beta_1'], & \text{Im } t < 0. \end{cases} \tag{51}$$

Terms of order $|t|^2/a^2$ and b^2/a^2 and higher have been neglected in the above expressions. The appearance of separate equations for the two situations Im $t > 0$ and Im $t < 0$ in the expression for w_1' is due to the fact that the modulus of the complex number $(1-t^2/a^2)^{\frac{1}{2}}$ is positive above the real axis and negative below it.

By taking the real parts of the expressions for w_1 and w_1' the polarization potentials can be found. In order to determine current distributions, however, we are more interested in the derivatives of S_1 and S_1'. These can be obtained directly from w_1 and w_1', for

$$\frac{\partial S_1}{\partial x} - i\frac{\partial S_1}{\partial y} = \frac{dw_1}{dt} = E(\alpha_1+i\beta_1). \tag{52}$$

Thus,

$$\partial S_1/\partial x = E\alpha_1; \qquad \partial S_1/\partial y = -E\beta_1. \tag{53}$$

Similarly,

$$dw_1'/dt = E(\alpha_1-i\beta_1'b/a); \tag{54}$$

hence,

$$\partial S_1'/\partial x = E\alpha_1; \qquad \partial S_1'/\partial y = E\beta_1'b/a. \tag{55}$$

The current distribution near the origin can now be obtained by substitution in (13) and (14). This gives

$$j_x = \partial J/\partial y = \sigma_1 E(\cos\phi-\alpha_1)+\sigma_2 E(\sin\phi+\beta_1) \tag{56}$$

$$j_y = -\partial J/\partial x = -\sigma_2 E(\cos\phi-\alpha_1)+\sigma_1 E(\sin\phi+\beta_1) \tag{57}$$

and

$$j_x' = \partial J'/\partial y = \sigma_1' E(\cos\phi-\alpha_1)+\sigma_2' E(\sin\phi-\beta_1 b/a) \tag{58}$$

$$j_y' = -\partial J'/\partial x = -\sigma_2' E(\cos\phi-\alpha_1)+\sigma_1' E(\sin\phi-\beta_1 b/a). \tag{59}$$

Of particular interest are the perturbation currents $\mathbf{i}, \mathbf{i}'$, that is, the additional currents flowing due to the enhancement of the ionization within the strip. They are defined by the equations

$$\mathbf{i} = \mathbf{j}-\mathbf{j}_q \tag{60}$$

$$\mathbf{i}' = \mathbf{j}'-\mathbf{j}_q \tag{61}$$

where

$$\mathbf{j}_q = \underset{\sim}{\Sigma}' \cdot \mathbf{E} \tag{62}$$

is the current density in the ionized gas when it contains no anomaly. Thus we have

$$i_x = E[(\sigma_1-\sigma_1')\cos\phi+(\sigma_2-\sigma_2')\sin\phi-\sigma_1\alpha_1+\sigma_2\beta_1] \tag{63}$$

$$i_x' = -E[\sigma_1'\alpha_1+\sigma_2'\beta_1'b/a] \tag{64}$$

$$i_y = i_y' = -E[\sigma_1'\beta_1'b/a-\sigma_2'\alpha_1]. \tag{65}$$

The equations for i_y and i_y' do not depend explicitly on x; this is to be expected since it is only valid in the neighborhood of the origin.

An important result which can be seen immediately from the equations (63), (64), and (65) is

$$i_x \gg i', i_y \tag{66}$$

since i_x is the only component which is not of order (b/a). Thus, the dominant perturbation current in a sheet of lightly ionized gas which contains a very long elliptical anomaly of greater ionization density is a linear current flow along the ellipse except near the end points. In fact, if we finally let $a \to \infty$ so that the ellipse becomes an infinitely long strip,

$$i_x \to \frac{E}{\sigma_1}[(\sigma_1^2+\sigma_2^2-\sigma_1\sigma_1'-\sigma_2\sigma_2')\cos\phi+(\sigma_1'\sigma_2-\sigma_1\sigma_2')\sin\phi] \tag{67}$$

and

$$i_y \to i_x' \to i_y' \to 0. \tag{68}$$

Since the components of the generalized conductivity matrix in a lightly ionized gas are all proportional to the ionization density (see equations (2), (3), and (4)) we can write

$$\frac{\sigma_\parallel}{\sigma_\parallel'} = \frac{\sigma_1}{\sigma_1'} = \frac{\sigma_2}{\sigma_2'} = \frac{n}{n'} = k \tag{69}$$

where k is the constant ratio of the ionization density, n, inside the anomaly to that outside, n'. Introducing k into (67), the expression for the perturbation current along the strip becomes

$$i_x = E(k-1)\sigma_3'\cos\phi = E_x(\sigma_3-\sigma_3') \tag{70}$$

where σ_3 and σ_3' are the Cowling conductivities of the gas inside and outside the strip. If the ionization density inside the strip is very much greater than that outside (but not so great that the gas ceases to become only lightly ionized) we can write $k \gg 1$ and hence

$$i_x \doteqdot \sigma_3 E_x. \tag{71}$$

4. APPLICATION TO THE IONOSPHERE

We have calculated the current systems in a thin sheet of partially ionized gas intersected perpendicularly by a constant magnetic field. We shall now attempt to modify this purely mathematical configuration so that it approxi-

mates to the actual physical conditions found in the ionosphere. It should then be possible to associate the currents calculated in the preceding section with current systems flowing in the ionosphere.

For simplicity the ionosphere will be considered as a neutral, lightly ionized gas composed of electrons, heavy positive ions, and neutral particles having the same mass as that of the positive ions. A region of auroral luminosity is one of greater ionization density and will therefore correspond to the anomalous regions introduced into the mathematical model. It is necessary that even within regions of auroral luminosity the ionosphere remains only lightly ionized; otherwise, the expressions for the conductivities $\sigma_\parallel$, σ_1, and σ_2 are no longer valid. Experimental evidence (e.g. Currie, Forsyth, and Vawter 1953) suggests that the maximum ionization density within an aurora is about $10^8/cm^3$. The density of neutral particles in the lower regions of the ionosphere is around $10^{12}/cm^3$. Thus even within the most highly ionized regions of the aurora, the atmosphere is only lightly ionized.

Although the representation of the ionosphere as a partially ionized gas appears to be very reasonable the configuration of the mathematical model does not directly correspond to the ionosphere intersected by the geomagnetic field. Also, certain assumptions which were made in the development of the mathematical theory will require investigation to see if they hold in the ionosphere.

Following are listed the features of the ionosphere which differ from the conditions assumed in our model:

(1) The earth and its atmosphere are not horizontal planes.

(2) The mass-velocity of the ionosphere (ionospheric wind velocity) is not constant; its magnitude and direction change considerably during the day.

(3) There is probably a vertical current incident on the ionosphere due to an impinging stream of solar corpuscles causing aurorae.

(4) The ionosphere is not "thin"; it has a finite thickness of over 200 km.

(5) The geomagnetic field is not perpendicular to the ionosphere; it is inclined at an angle given by the magnetic dip at that point.

(6) An ionization anomaly in the ionosphere does not necessarily move with the ionospheric wind velocity; an aurora is observed to be stationary or to move with a velocity relative to the wind.

Each of the above items will be investigated in order to establish what modifications, if any, are required before the mathematical results can be applied to the ionosphere.

The Curvature of the Earth

As in this work we are only concerned with local current systems and their related local magnetic disturbance, as distinct from world-wide effects, we are restricting our observations to a small area of the earth's surface. In this case the earth and ionosphere can be considered as horizontal planes to a good approximation.

Ionospheric Wind Velocity

Although the ionospheric wind velocity $\mathbf{v}$ is not constant, the only com-

ponents of its periodic variation which are important are the diurnal and semidiurnal ones. The change in wind velocity, which according to radio measurements (Briggs and Spencer 1954) is principally semidiurnal, is negligible during the period of time in which transient ionospheric currents grow and decay. The wind velocity can thus be taken as having constant value $\mathbf{v}$, even though both the magnitude and direction of $\mathbf{v}$ will have different values at different times of day.

Incident Vertical Currents

In the gas sheet of the mathematical model it was assumed that an anomaly of ionization density merely existed; the cause of the enhancement was not discussed. In the ionosphere, however, one must take into account the cause of aurorae, for according to most auroral theories the ionizing agent is a solar corpuscular stream incident on the earth's atmosphere and as such constitutes a vertical electrical current unless the stream is electrically neutral. In particular, such a current will affect equation (7) and will also possess a magnetic field which might be responsible for a significant part of the magnetic disturbance vector measured at the earth's surface.

The effect of the incident vertical current on the validity of equation (7) need concern us no further, if we suppose it to be completely absorbed by collisions. In this case, incident particles are driven back up the lines of force after coming to rest, thereby making no contribution to horizontal current flow. The three dimensional equation of continuity clearly reduces to equation (7) in this situation.

To ascertain whether the magnetic field of the vertical current is important or not an order of magnitude calculation was carried out. The current sheet of diminishing current density was replaced, for mathematical simplicity, by an infinite sheet of constant density, the current system being closed at infinity. This sheet actually has a magnetic field greater than that required but this is immaterial as we are interested primarily in an upper bound for the magnetic field associated with the solar corpuscular current sheet. Indeed, if the solar particles accelerate back up the lines of force out of the earth's atmosphere after coming to rest, then the effective vertical current and its magnetic field are substantially reduced even further. The constant current density of the sheet was taken as 10^{-3} amp/cm. This is consistent with an auroral arc width of 10 km and the estimates of either an incident electron flux given by Vegard (1955) or of an incident proton flux given by Chamberlain (1954), whichever might be the primary ionizing agent. It was found that the magnitude of the horizontal magnetic disturbance H at the surface of the earth in the neighborhood of the arc is such that $H < 10\pi\gamma(1\gamma = 10^{-5}$ gauss). Thus H is at most only of the order of magnitude of the S_q magnetic field and is therefore negligible compared with the much greater magnetic disturbances associated with auroral arcs.

The Thickness of the Ionosphere

It was argued in Section 3 that currents in a sheet of gas flowed horizontally, all vertical flow being impeded by a vertical polarization field. In fact, with a

perpendicular magnetic field only a transverse electric field $\mathbf{v}\times\mathbf{H}$ was effective so that vertical flow would have been absent in any case. Were there no ionization anomaly in the ionosphere, the current flow in the ionosphere could be obtained by considering it as a series of horizontal sheets, each of uniform conductivity, lying one on top of the other. On the assumption that the wind velocity is independent of height, the equations would be exactly the same as those for a thin sheet with the conductivities σ replaced by corresponding height-integrated conductivities, the integrations being throughout the conducting regions of the ionosphere.

When the ionosphere is aurorally active and therefore contains an ionization anomaly, the situation is complicated by the presence of the electrostatic polarization field caused by the accumulation of charge on the boundary of the anomaly. If we again consider the ionosphere to be a series of thin layers, one on top of the other, the varying ionization density (and hence conductivity) from layer to layer causes different charge densities to accumulate on the boundaries at different heights, thereby adding a vertical component to the polarization field $-$grad S. Thus, since there is a vertical conductivity $\sigma_\parallel$ in the ionosphere, a current flows up the boundary of the arc and the assumption that div $\mathbf{j}$ vanishes in each horizontal plane is no longer valid.

However, an order of magnitude calculation of the charge distribution on the sides of the arc revealed that the vertical current leakage from any horizontal layer was at least a factor 10^3 smaller than the steady state horizontal current flowing in the layer. Vertical flow can therefore be considered negligible, not only in the steady state, but during the build-up process also. Thus, in each horizontal plane div $\mathbf{j}$ is essentially zero, and currents are induced in each layer of the ionosphere according to the equations of Section 3, and can be height-integrated directly. In particular, the height-integrated perturbation current density along an auroral arc is given by s_x where

$$s_x = \int i_x dh = E_x \int (\sigma_3 - \sigma_3')dh. \tag{72}$$

The Inclination of the Geomagnetic Field

When the magnetic field makes an angle I with the plane of the gas sheet, it is a simple matter (Chapman 1956) to show that the correspondingly modified forms of equations (13) and (14) are

$$\partial J/\partial y = -\lambda_1\sigma_1\partial V/\partial x - \lambda_2\sigma_2\partial V/\partial y \tag{73}$$

$$\partial J/\partial x = -\lambda_2\sigma_2\partial V/\partial x + \lambda_3\sigma_1\partial V/\partial y \tag{74}$$

where

$$\lambda_1 = (\sigma_3 \cos^2 I + \sigma_\parallel \sin^2 I)/C \tag{75}$$

$$\lambda_2 = (\sigma_\parallel \sin I)/C \tag{76}$$

$$\lambda_3 = \sigma_\parallel/C \tag{77}$$

$$C = \sigma_1 \cos^2 I + \sigma_\parallel \sin^2 I. \tag{78}$$

Thus the inclination of the magnetic field merely involves the introduction

of the correction factors $\lambda_{1,2,3}$. In auroral latitudes $I \doteqdot 80°$ and in all regions of the ionosphere above 90 km, $\sigma_1 \ll \sigma_\parallel$. Under these conditions, it was found that $1 < \lambda_1 < 1.03$, $\lambda_2 \doteqdot 1.01$, and $\lambda_3 \doteqdot 1.03$. In view of the fact that with presently available numerical data calculations of ionospheric conductivities involve errors of up to 10%, it is clear that in latitudes where auroral arcs occur, only insignificant errors are introduced by taking the geomagnetic field to be perpendicular to the ionosphere.

The Motion of Aurora

Until now it has been tacitly assumed that the region of greater ionization density moves with the local wind velocity. In fact the equations developed in Section 3 refer to quantities measured in a co-ordinate system moving with the velocity **v**. This does not affect the expressions for the current densities which remain unaltered when transformed to a co-ordinate system fixed with respect to the earth, but care is needed in transforming polarization fields and velocities. If the incoming ionizing agent itself (and hence the aurora) is drifting with velocity **v**, the above requirements will be met. In general, however, the velocity of auroral motions differs from that of the local wind velocity (Kim and Currie 1958).

Let us consider the physical situation when the region being ionized is moving with a velocity different from that of the local wind. For the sake of argument, we will take both velocities to be in the same direction with the auroral velocity the greater of the two. Consider the trailing boundary of the moving strip which contains an accumulation of, say, negative charge. When the ionizing agent is displaced the negative charge will be left isolated and will decay by recombining with the positive ions in the new boundary of the ionized strip immediately in front of them, leaving a net accumulation of negative charge on the new boundary. This process will continue as the aurora advances so that the negative charge concentration is effectively carried along with the boundary of the strip. Similar reasoning shows that positive charge will be carried along with the leading edge so that in effect, the polarization field moves with the aurora, that is, it is defined with respect to a reference system moving with the velocity of the aurora. Thus, referred to these axes the total electric field is $(\mathbf{u}\times\mathbf{H}-\text{grad}\, S)$, where **u** is the velocity of the aurora. This transforms into $(\mathbf{v}\times\mathbf{H}-\text{grad}\, S)$ referred to axes moving with the wind velocity. Thus all our results remain valid for moving aurora providing only that our mathematical idealization of the boundary as a line contour is still acceptable, and that div **j** is still zero throughout the region.

In practice, of course, the boundary of the anomaly will be diffuse, the concentration of charge being spread over a finite distance. It is therefore a necessary condition that this distance be small in comparison with the total width of the strip. The maximum possible velocity of the aurora relative to the ionized particles is $(u+v)$. Thus, if t is the relaxation time of the ionization decay, the aurora will have travelled a distance $(u+v)t$ relative to the particles before appreciable recombination will have taken place. We therefore, require the condition $(u+v)t \ll d$ to be satisfied, where d is the width of the arc. Measurements on auroral movements by Kim and Currie (1958) suggest

that the average N.–S. velocity of auroral arcs is about 10^6 cm/min; ionospheric winds are of the order 10^5 cm/min. Taking 10 km as an average auroral arc width, the above condition requires $t \ll 1$ min. This is satisfied, as far as can be ascertained, by recombination reactions taking place within an aurora. For instance, the time for 90% recombination for the reaction $N_2^+ + e \rightarrow N + N$ is about 0.1 sec (Biondi and Brown 1949). It is therefore concluded that the assumption that the boundary of a moving aurora is sharp, is not too drastic an approximation.

It must be shown also that div $\mathbf{j}$ remains zero when the auroral arc has a velocity $\mathbf{u}$. In this case, referred to axes moving with the wind, the charge density ρ becomes time dependent taking the form

$$\rho = \rho(|\mathbf{r} - \mathbf{v}'t|) \tag{79}$$

where $\mathbf{v}' = \mathbf{u} - \mathbf{v}$ is the velocity of the aurora relative to the wind. Thus,

$$\text{div } \mathbf{j} = -\partial\rho/\partial t = -\mathbf{v}' \text{ grad } \rho = -\text{div } (\rho\mathbf{v}') \tag{80}$$

since div $\mathbf{v}' = 0$. Hence, if we define a new "current" density vector $\mathbf{j}'$ by the relation

$$\mathbf{j}' = \mathbf{j} + \rho\mathbf{v}', \tag{81}$$

we have

$$\text{div } \mathbf{j}' = 0. \tag{82}$$

Order of magnitude calculations indicated that $|\rho\mathbf{v}'|$ was at least a factor 10^2 smaller than $\mathbf{j}$; hence by (81), $\mathbf{j}' \doteqdot \mathbf{j}$ and equation (82) reduces to div $\mathbf{j} \doteqdot 0$, as required for the mathematical theory to remain valid for moving aurorae.

5. SUMMARY

It has long been assumed that a line current flows along an auroral arc. The evidence supplied by magnetic records points very strongly to this fact. For instance, Stagg and Paton (1939) and Heppner (1954) found that the angle of elevation of an auroral arc from any point agrees very well with the elevation of the perpendicular to the magnetic disturbance vector measured at the same point. A more striking indication of an auroral line current is the reversal of the Z-component of magnetic disturbance as one passes underneath an arc. This has also been observed by Heppner, as well as by many others.

From a theoretical investigation of the current distribution in a partially ionized gas containing an ionization anomaly, it has been shown in this paper how the auroral line current could be produced by dynamo action in the ionosphere. The theory has also provided an expression (equation (72)) for the magnitude of the height-integrated line current density.

In a subsequent paper, order of magnitude calculations for the theoretical line current will be presented and some of the results predicted by the theory will be compared with observational evidence.

ACKNOWLEDGMENTS

One of us (J. T. W.) gratefully acknowledges financial assistance in the form of a National Research Council Studentship.

REFERENCES

BAKER, W. G. and MARTYN, D. F. 1953. Phil. Trans. Roy. Soc. London, A **246**, 281.
BIONDI, M. A. and BROWN, S. C. 1949. Phys. Rev. **76**, 1697.
BRIGGS, B. H. and SPENCER, M. 1954. Repts. Progr. in Phys. **17**, 245.
CHAMBERLAIN, J. W. 1954. Astrophys. J. **120**, 360.
CHAPMAN, S. 1956. Nuovo Cimento Suppl. (10), **4**, 1385.
COWLING, T. G. 1933. Monthly Notices Roy. Astron. Soc. **93**, 90.
——— 1945. Proc. Roy. Soc. A, **183**, 453.
CURRIE, B. W., FORSYTH, P. A., and VAWTER, F. E. 1953. J. Geophys. Research, **58**, 179.
DUNGEY, J. W. 1958. Cosmic electrodynamics (Cambridge University Press, Cambridge).
HEPPNER, J. P. 1954. Ph.D. Thesis, California Institute of Technology, California.
KIM, J. S. and CURRIE, B. W. 1958. Can. J. Phys. **36**, 160.
MARTYN, D. F. 1948. Nature, **162**, 142.
——— 1953. Phil. Trans. Roy. Soc. London, A **246**, 306.
MEEK, J. H. 1955. Ph.D. Thesis, University of Saskatchewan, Saskatoon, Saskatchewan.
PEDERSEN, P. O. 1927. Danm. Naturvid. Samf. A **15**, a/b.
STAGG, J. M. and PATON, J. 1939. Nature, **143**, 941.
VEGARD, L. 1955. Geofys. Publikasjoner, **19**, No. 4.

A THEORY OF IONOSPHERIC CURRENTS ASSOCIATED WITH AURORAE. II[1]

J. T. WEAVER[2] AND R. SKINNER

ABSTRACT

The average ionospheric current flowing along a long homogeneous arc, is calculated numerically on the basis of the theory developed in Part I. This is compared with the auroral current necessary to produce the observed magnetic disturbance at Saskatoon (52.1° N., 106.6° W.) and Flin Flon (54.7° N., 102.0° W.) for an arc which satisfies the conditions required by the theory. A good order of magnitude agreement between the two values is obtained.

The theory also shows that, in general, the magnitude of the line current is proportional to the intensity of the arc, but that when the ionospheric wind is directed along the arc, the line current vanishes. Thus a simple explanation of the occurrence of arcs with no associated magnetic disturbance is provided.

A relationship between the average magnetic disturbance due to arcs and the ionospheric wind velocity is also established. The hourly variation of magnetic disturbance during aurorally active hours at Saskatoon and Flin Flon is shown to predict ionospheric wind velocity variations which agree well with those obtained by radio measurements.

1. INTRODUCTION

In Part I (Weaver and Skinner 1960), a theoretical expression for the ionospheric current associated with a long homogeneous auroral arc was developed. It was found that under the assumed conditions, a linear current flow was directed along the arc, its magnitude away from the ends being given by

$$s_x = E_x \int (\sigma_3 - \sigma_3') \, dh \tag{1}$$

where σ_3, σ_3' are the Cowling conductivities within and outside the arc, respectively, and E_x is the horizontal dynamo electric field in the x-direction of the arc. (Since arcs are generally aligned in an east–west direction, we shall henceforth refer to the x-direction as eastward along the arc. The y-direction is then northward, perpendicular to the arc.) Important deductions can be made from this result, and it is desirable to attempt to compare these with actual geomagnetic and auroral observations. Some of the comparisons which have already been made with data collected at Saskatoon (52.1° N., 106.6° W.) and Flin Flon (54.7° N., 102.0° W.) are presented in this paper.

2. NUMERICAL MAGNITUDE OF AVERAGE AURORAL CURRENTS

Equation (1) can be written in the form

$$s_x = (K_3 - K_3') \, E_x \tag{2}$$

where $K_3 = \int \sigma_3 dh$ and $K_3' = \int \sigma_3' dh$ are the height-integrated Cowling conductivities, the integrations being carried throughout the conducting

[1]Manuscript received May 2, 1960.
Contribution from the Physics Department, University of Saskatchewan, Saskatoon, Saskatchewan.
[2]Now at the Department of Mathematics, University of Saskatchewan, Saskatoon, Saskatchewan.

regions of the ionosphere. Thus in order to calculate an average value for the numerical magnitude of s_x it is first necessary to obtain values for K_3 and K_3' from the best available ionospheric data.

The most straightforward method of calculating these values is to plot curves of σ_3 and σ_3' against altitude and to use a numerical integration. The height variation of the Cowling conductivity per electron–ion pair has been calculated by several authors (e.g. Baker and Martyn 1953; Chapman 1956); it was recalculated for the present work making use of the ionospheric data given by Bates and Massey (1951) and with the same assumptions as those made by Baker and Martyn. For details we refer the reader to the papers of these authors.

Before proceeding to calculate the actual values of σ_3 and σ_3' at various altitudes, it is necessary to know the height distribution of the ionization densities along vertical lines passing through both aurorally active and unexcited regions of the ionosphere. We shall call these distributions $N = N(h)$ and $N' = N'(h)$ respectively.

In recent years rocket flight measurements have shown that the normal electron density variation with altitude in the ionosphere is a much smoother curve than had been originally assumed. From daytime rocket measurements at White Sands, New Mexico, Seddon, Pickar, and Jackson (1954) report that the ionosphere remains heavily ionized throughout the 100–200 km region. No existence of sharply defined layers was found. These results have been confirmed by more recent measurements (Jackson and Seddon 1958). We adopt here a smoothed-out version of the electron-distribution curve given in the 1954 paper by assigning N' the values 0, 10^4, 10^5, 2.1×10^5, 1.9×10^5, and 2.5×10^5/cm^3 at the heights 80, 90, 100, 160, 200, and 250 km respectively. The variation with height between these levels is taken to be uniform; thus minor fluctuations on the experimental graph are disregarded. The adoption of this model for N' is open to some criticism since it is based on data pertaining to daytime ionospheric conditions above New Mexico. Nighttime ionospheric densities at auroral latitudes could differ from the chosen values by as much as a factor of 10. A graph of the adopted height distribution of N' is shown in Fig. 1.

In order to determine the variation of N with altitude, the distribution of ionization within an auroral arc must be determined. Owing to the uncertainty of the assumptions required for the derivation of a theoretical distribution, it is assumed here that ionization density is proportional to auroral light intensity and we therefore adopt the observed intensity distribution for arcs as giving also the ionization density distribution. The standard luminosity curve of Vegard (1921) was used, as more recent measurements of luminosity (e.g. Harang 1946*a*) give essentially the same distribution. The base of Vegard's curve is taken to be at 100 km, the mean altitude of the lower limit of auroral arcs. If the numerical value of the maximum density in an arc is known (corresponding to the peak on the luminosity curve) the horizontal axis can be scaled off accordingly in units of ionization density.

Information concerning the maximum ionization density in auroral forms is at present in an uncertain state. It appears, however, on the evidence of

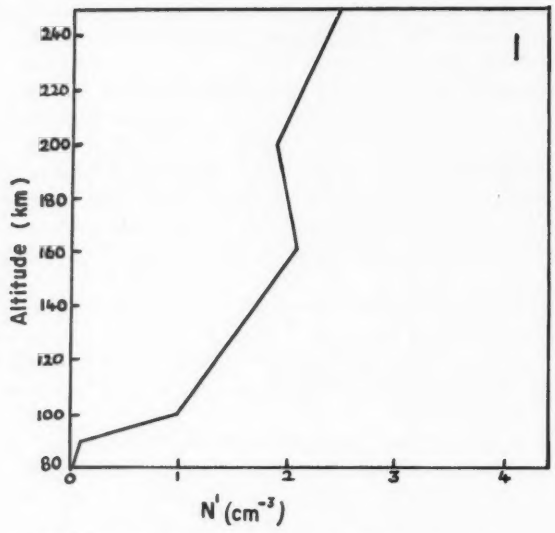

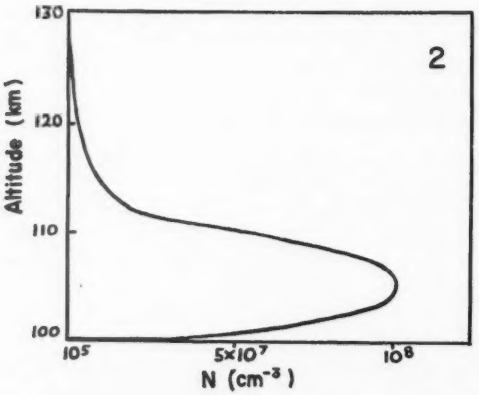

FIG. 1. Adopted electron density distribution (N') in the ionosphere.
FIG. 2. Electron density distribution (N) within an auroral arc.

radar measurements, that densities of the order $10^8/cm^3$ exist in aurorae (see e.g. Currie, Forsyth, and Vawter (1953)); for the present calculation this seems to be a reasonable value to adopt. (Forsyth (1959) has pointed out that the figure $10^8/cm^3$ probably refers to isolated anomalies of high ionization existing within an aurora, and that the mean maximum ionization density may be smaller.)

Figure 2 illustrates the adopted density distribution, namely, Vegard's luminosity curve scaled such that the peak ionization density has a value

$10^8/cm^3$, and with the cutoff at an altitude of 100 km. The graph represents the distribution N only within the aurora; above and below the arc normal ionospheric conditions, specified by Fig. 1, exist. Thus we can write

$$N(h) = N'(h), \qquad (h \leqslant 100, 130 \leqslant h) \tag{3}$$

where h is measured in km.

The Cowling conductivity distributions σ_3 and σ_3' corresponding to densities N and N' respectively are shown in Fig. 3. It can be seen from the graph that the layer in which σ_3 exceeds 1% of its peak value is only 20 km wide, the

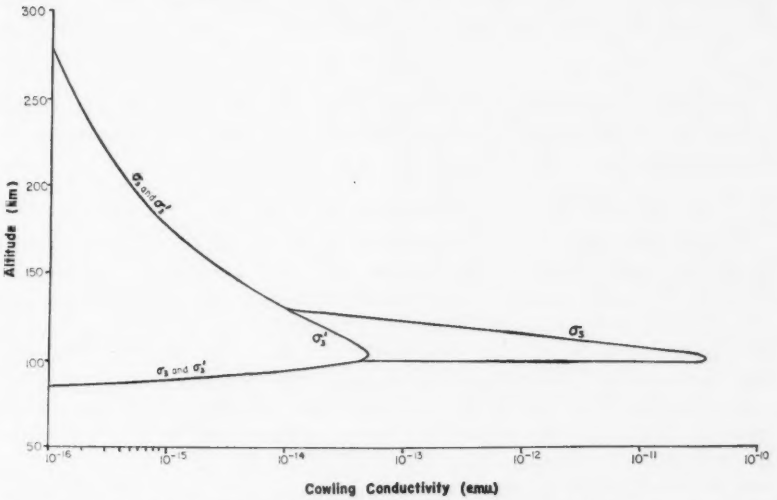

FIG. 3. Variation with altitude of Cowling conductivity for normal (σ_3') and aurorally active (σ_3) ionospheres.

peak occurring at an altitude of about 105 km. The effective layer for the Cowling conductivity in the ionosphere when an auroral arc is present is thus extremely thin, and is restricted to the lower part of the E-region. Under normal ionospheric conditions the maximum value of the Cowling conductivity occurs at approximately the same altitude but is reduced a thousand fold in magnitude.

An approximate numerical integration yields

$$K_3 = 3.3\times10^{-5} \text{ e.m.u. cm}$$

$$K_3' = 1.4\times10^{-7} \text{ e.m.u. cm.}$$

These values show that $K_3 \gg K_3'$ and hence equation (2) becomes approximately

$$s_x = K_3 E_x. \tag{4}$$

It will be recalled that $E_x = -v_y H$ where v_y is the northward component of the ionospheric wind velocity perpendicular to the arc and H is the geomagnetic field. Thus if b is the horizontal width of the arc, the total perturbation current I flowing eastwards along the arc is given by

$$I = -bK_3 v_y H. \tag{5}$$

According to Briggs and Spencer (1954) the maximum value of v_y at Cambridge, England, during the night hours is about 5×10^3 cm/sec and since it has a semidiurnal sinusoidal variation its average value is approximately two-thirds as large. Since Saskatoon is at approximately the same latitude as Cambridge, we adopt the same value for v_y in the present calculation. Taking $b = 10$ km, $H = 0.6\ \Gamma$ and using the above value for K_3 we obtain from (5)

$$I \sim 10^6 \text{ amp.}$$

It follows from the discussion of the graphs in Fig. 3 that this current is restricted to a relatively thin region of the ionosphere in the lower part of the E-region, that is near the base of the arc.

3. COMPARISON WITH AURORAL AND MAGNETIC RECORDS

It is not difficult to devise a method of testing whether the theoretically predicted magnitude of I is consistent with data collected at two stations situated in the vicinity of an auroral arc and which are equipped with magnetometers and all-sky cameras. The exact location of the auroral arc can be determined from the all-sky photographs and the magnitude of the auroral line current which would produce the observed magnetic disturbances can then be calculated, taking into consideration the effect of induced earth currents. On the assumption that these currents can be replaced by an equivalent line current at some depth below the surface of the earth, some simple geometric reasoning shows that

$$2I = r_1 r_2 \left[\frac{\Delta H_1 \Delta Z_2 \cot e_1 + \Delta H_2 \Delta Z_1 \cot e_2}{r_1(\Delta Z_1 + \Delta H_1 \cot e_1) \cos e_2 + r_2(\Delta Z_2 - \Delta H_2 \cot e_2) \cos e_1} \right] \tag{6}$$

where subscripts 1 and 2 refer to the two stations, r and e are the distance and elevation of the arc respectively, and ΔH and ΔZ are the horizontal (northward) and vertical (downward) components of the magnetic disturbance vector.

Unfortunately, in order to carry out such a comparison three very stringent conditions must be satisfied. These are:

(1) the arc must be long and situated such that the magnetic stations are near its center;

(2) the arc must be the only form of auroral activity present at the time in question;

(3) apart from the magnetic disturbance associated with the arc, the day must be, on the whole, magnetically quiet.

Clearly (1) must be satisfied in order that the requirements of the mathematical theory be fulfilled. Conditions (2) and (3) are necessary if one is to

know, beyond doubt, that the registered magnetic disturbance is associated with the observed arc. Thus, although the method is simple, the number of arcs which lend themselves to analysis in this manner is very small.

Magnetometers and all-sky cameras have been operating at Saskatoon and Flin Flon for a number of years. Both stations lie near the auroral zone and are only about 400 km apart so that the same auroral arc is often recorded by both cameras. An examination of the records from these two stations revealed an arc for which conditions (1) to (3) above were well satisfied. This occurred at 0931 G.M.T. on March 14, 1956.

Figure 4 illustrates the essential steps in the analysis of this arc. It represents a map of the area with the position of the arc (assumed to be at an altitude of

FIG. 4. Geographical location of the arc of March 14, 1956.

100 km) sketched in, and showing also the magnetic disturbance vectors registered at each station. Substitution of the relevant quantities in equation (6) yielded

$$I = 1.2\times10^5 \text{ amp.}$$

This value agrees extremely well with the predicted order of magnitude for the average auroral current of 10^6 amp. The fact that it is somewhat smaller is exactly what one would expect since the influence of the return current has been completely ignored in the theoretical treatment where it was assumed the arc was infinitely long. For a finite length, the return current densities are small compared with the auroral current (they are of order b/a, see equation (64), Part I), but over large distances their integrated effect becomes important.

It is not easy to make extensive comparisons of this type owing to the stringent conditions required. However, the theory can be tested in a more indirect way by considering other predictions which can be extracted from equation (5).

4. ARCS WITH NO MAGNETIC DISTURBANCE

The occurrence of arcs with little or no associated magnetic disturbance has been noticed since interest in auroral studies first began. Vegard (1916) drew attention to this fact over 40 years ago, and observed that even arcs with relatively strong luminosity could possess this characteristic. He concluded that aurorae in general give rise to only relatively small magnetic effects and are not directly related to strong disturbances. However, investigations by Harang (1946*b*), Murcray (1958), and others indicate that an increase in auroral luminosity leads to an increase in magnetic disturbance, a fact which contradicts Vegard's conclusions.

The apparent discrepancy can be very simply explained. Equation (5) shows that, in general, the auroral current I is indeed proportional to the auroral intensity, since K_3 is directly proportional to the ionization density within the arc, and hence to its luminosity. However, if $v_y = 0$, we obtain $I = 0$ irrespective of the magnitude of K_3. Thus, even a very bright arc could produce zero magnetic disturbance if the ionospheric wind happened to be directed along the arc at that time. The appearance of such arcs is therefore not a strange phenomenon; it is a natural consequence of the dynamo theory for auroral currents.

It will be noticed that the explanation offered here applies only to auroral forms whose lengths are large compared with their widths. It is therefore interesting to note that Vegard observed only arcs, bands, and draperies possessing this feature although he generalized his conclusions to all types of aurorae.

It was not possible to test this explanation experimentally since no information (apart from average results) on the direction of the ionospheric wind at the time of occurrence of an arc was available. However, an examination of the records showed that auroral forms without an associated magnetic disturbance were by no means a rare occurrence. Seventeen such cases were found in the Flin Flon records for the period December 1955 to July 1957 and 12 at Saskatoon for the period December 1955 to April 1957. (For the purposes of this examination any disturbance of less than 20 γ was considered negligible.)

5. MEAN MAGNETIC DISTURBANCE

Consider a long homogeneous auroral arc situated at a distance r from some station. Let the orientation of the arc be such that the angle between geomagnetic north and the direction of the arc is α, measured in a clockwise direction. Then the magnitude of the magnetic disturbances vector $\Delta\mathbf{F}$, directed northwards in sense, is given by

$$\Delta F = 2I/r \tag{7}$$

where I is given by (5). Thus, if ΔH is the horizontal component of this disturbance

$$\Delta H = 2hI/r^2 \tag{8}$$

where h is the height of the aurora. That is,

$$\Delta H(t) = -cv_y(t)/r^2 \tag{9}$$

where $c = 2hbK_3h$, and the variable t has been introduced to indicate which quantities are dependent on local time. If $\Delta X(t)$ is the northward component of $\Delta H(t)$, we have

$$\Delta X(t) = -cv_y(t) \sin \alpha/r^2. \tag{10}$$

It is now assumed that the variables v_y, r, and α are statistically independent. Thus by taking the average over many arcs occurring on different days at the time t, and noting that $\overline{(1/r^2)}$ and $\overline{\sin \alpha}$ must be independent of time, (10) can be written as

$$\overline{\Delta X(t)} \propto -\overline{v_y(t)}. \tag{11}$$

Our assumption of statistical independence may not be entirely true, for although Jensen and Currie (1953) report no systematic diurnal variation of the orientations of arcs, there is on the other hand, reason to suppose that the latitude of arcs is correlated with local time (Vegard 1912).

Equation (11) implies that the average X-component of the magnetic disturbance field due to auroral arcs varies with local time in the same way as the southward component of the average ionospheric wind velocity.

In order to test this conclusion, an analysis of the mean magnetic disturbance for those hours of the night during which an auroral arc was present was made. The maximum value of the X-component of magnetic disturbance for each hour of auroral activity (in the form of long arcs) was recorded for the years 1956 and 1957 at both Saskatoon and Flin Flon stations. The magnitude of the disturbance was indicated by a K-index which was devised by Meek (1956) for Saskatoon; this index is also suitable for Flin Flon. Since the S_q variation in this region is only of the order 10 γ its effect was ignored, and the deviation of the trace on the magnetometer chart from its normal position was taken as a direct measurement of the disturbance associated with the aurora. (The magnetometers actually record the geographic, not the geomagnetic components, but the difference is slight.)

The variation with local time of the mean K-index (averaged for each hour over the 2-year period) is shown in histogram form in Fig. 5 for both Saskatoon and Flin Flon. Smooth curves have been superimposed on the histograms.

Equation (11) predicts that this variation should be directly proportional to the variation of the southward component of the ionospheric wind. The idealized semidiurnal variations of the north–south ionospheric wind, based on experimental data obtained by radio methods at Cambridge (Briggs and Spencer 1954) and Ottawa (Chapman 1953) are also shown for comparison in Fig. 5.

Although the nighttime parts of these curves are essentially extrapolations of daytime measurements, they are confirmed by a limited number of measurements on sporadic-E ionization movements made during the night. It can be

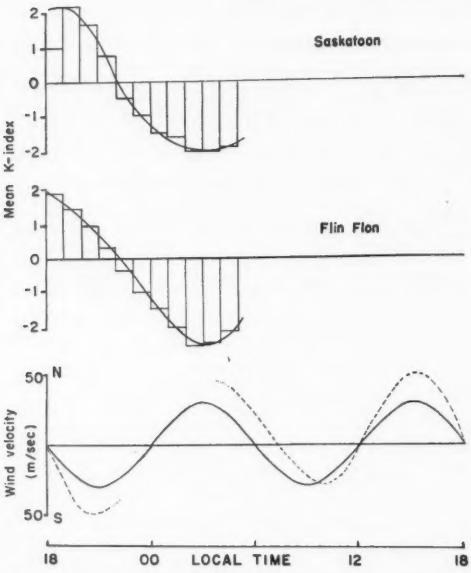

FIG. 5. Idealized variations with local time of the mean K-index and north–south component of the ionospheric wind. ——— Briggs and Spencer (1954); --- J. H. Chapman (1953).

seen that these curves are consistent with the nighttime wind variations predicted by equation (11) from the variation of the mean K magnetic index. The average wind velocity is southward before midnight when the mean magnetic disturbance is positive, and northward when it is negative after midnight. It is not possible, of course, to compare the amplitude of the curves without a knowledge of the distribution of the geographical position of the arcs, but it has already been established in Section 3 that there is a good order of magnitude agreement, at least for the particular arc examined.

The slight phase difference of about $1\frac{1}{2}$ hours between the curves is not considered serious as the radio measurements of ionospheric movements during the night are not sufficiently numerous to establish the precise hour of reversal of the north–south wind.

6. SUMMARY

In this paper, a further discussion of the dynamo theory for auroral currents (developed in Part I) has shown that the theory explains several observed auroral phenomena. In particular, the following results have been noted.

1. The theory explains the line current flowing along an auroral arc.

2. Calculations have shown that this current is generally confined within a region less than 20 km in vertical extent from the base of the arc.

3. In general, the intensity of magnetic disturbance associated with an arc is proportional to the intensity of the arc.

4. At times when the ionospheric wind is directed along the arc, however, there will be no associated magnetic effects, regardless of the intensity of the arc.

5. The average horizontal north-component of magnetic disturbance associated with arcs varies in time with the south-component of the local average ionospheric wind.

Although the conditions involved in the mathematical development prevented an extensive comparison of these results with recorded magnetic and auroral data, for the one particular arc examined there was a good order of magnitude agreement between the theoretical auroral current and the observed associated magnetic disturbance. Also, an examination of magnetic data showed that average wind variations were consistent with those found experimentally by radio methods. When a better experimental knowledge of the behavior of ionospheric winds is known, it should be possible to test the theory more fully.

ACKNOWLEDGMENTS

One of us (J. T. W.) gratefully acknowledges financial support from a National Research Council Studentship and later from the Defence Research Board. The assistance of Mr. J. W. Scrimger in examining and analyzing the auroral and magnetic data was much appreciated.

REFERENCES

BAKER, W. G. and MARTYN, D. F. 1953. Phil. Trans. Roy. Soc. London, A **246**, 281.
BATES, D. R. and MASSEY, H. S. W. 1951. J. Atmospheric and Terrest. Phys. **2**, 1.
BRIGGS, B. H. and SPENCER, M. 1954. Repts. Progr. in Phys. **17**, 245.
CHAPMAN, J. H. 1953. Can. J. Phys. **31**, 120.
CHAPMAN, S. 1956. Nuovo Cimento Suppl. (10), **4**, 1385.
CURRIE, B. W., FORSYTH, P. A., and VAWTER, F. E. 1953. J. Geophys. Research, **58**, 179.
FORSYTH, P. A. 1959. Private communication.
HARANG, L. 1946*a*. Terrestrial Magnetism, **51**, 381.
——— 1946*b*. Terrestrial Magnetism, **51**, 353.
JACKSON, J. E. and SEDDON, J. C. 1958. J. Geophys. Research, **63**, 197.
JENSEN, R. E. and CURRIE, B. W. 1953. J. Geophys. Research, **58**, 201.
MEEK, J. H. 1956. A magnetic disturbance index for Saskatoon, Report from the Division of Physical Research (Geophys.), D.R.B. Ottawa.
MURCRAY, W. B. 1958. Sci. Rept. No. 2, AF 19(604)-1859, University of Alaska.
SEDDON, J. C., PICKAR, A. D., and JACKSON, J. E. 1954. J. Geophys. Research, **59**, 521.
VEGARD, L. 1912. Phil. Mag. **23**, 211.
——— 1916. Ann. Phys. **50**, 853.
——— 1921. Phil. Mag. **42**, 47.
WEAVER, J. T. and SKINNER, R. 1960. Can. J. Phys. **38**. This issue.

SCATTERING OF RADIO WAVES BY AN IONIZED GAS IN THERMAL EQUILIBRIUM[1]

J. A. FEJER

ABSTRACT

A theory is developed for the scattering of radio waves by density fluctuations which exist in an ionized gas in thermal equilibrium.

Expressions for the frequency power spectrum of the scattered waves are obtained. These expressions make it possible to interpret the results of observations of this type of scattering from the ionosphere in terms of electron density and temperature.

It is shown that if the characteristic scale of the scattering irregularities (this scale depends on the wavelength of the incident radio wave and the scattering angle) is much greater than the Debye length then the width of the spectrum of the scattered signal is determined by the thermal velocities (and the collision frequencies if the latter are sufficiently high) of the positive ions, rather than of the electrons.

If the characteristic scale is greater than the Debye length then for low collision frequencies the spectrum is flat-topped, with two slightly raised shoulders situated symmetrically above and below the frequency of the incident wave. For high collision frequencies the spectrum has only one maximum situated at the frequency of the incident wave.

1. INTRODUCTION

Gordon (1958) has recently pointed out that scattering of radio waves from an ionized gas in thermal equilibrium may be detected by a powerful radar. His analysis was based on the assumption that the electrons were in random thermal motion of the same type as the motion executed by the neutral particles. On this assumption he was able to calculate the scattering cross section and the power spectrum of scattering.

Bowles (1958, 1959) finds that if a powerful radar is beamed vertically upwards, a weak noiselike return is observed from ionospheric heights. Bowles' observations show that the amount of power contained in these backscattered waves is in approximate agreement with Gordon's predictions but that the power is spread over a much narrower frequency band than Gordon predicted.

Bowles (1959) also gives a tentative theoretical explanation of his experimental results. His explanation makes use of the work of Pines and Bohm (1952), who considered the density fluctuations in an electron gas in the presence of a uniform positive charge density. Bowles (1959) points out that the positive charge density is not uniform but fluctuates as a result of the random thermal motion of positive ions. The electrostatic forces considered by Pines and Bohm suppress the fast spontaneous fluctuations of electron density but the same electrostatic forces cause slow fluctuations of electron density which neutralize the slow spontaneous fluctuations of ion density. This explains the observed narrow spectrum.

[1]Manuscript received April 19, 1960.
Contribution from the D.R.B. Theoretical Studies Group, Defence Research Board, Ottawa, Canada.

In Section 2 of this paper the treatment of Pines and Bohm is modified by removing the restrictive assumption of a uniform positive charge density. The scattered power is then calculated with the aid of the revised treatment. The results of this analysis agree with the conclusions of Kahn (1959), who used slightly different methods in his calculation.

In Sections 3 and 4 of the present paper the power spectrum of the scattered signal is calculated for a number of different approximations.

2. CALCULATION OF THE SCATTERED POWER

Consider a medium in which the mean dielectric constant is ϵ. Assume further that there are irregular deviations $\Delta\epsilon$ from the value ϵ within a finite volume V. Then at a very long distance R from the volume V the electric field E_s of the waves scattered by these irregularities from an incident plane wave, the electric field of which is $E_0 \exp[i(\omega_0 t - \mathbf{k}_0 \cdot \mathbf{r})]$ is given by Booker and Gordon (1950) as

$$(1) \qquad E_s = \frac{E_0 k^2 \sin\gamma \exp[i(\omega_0 t - kR)]}{4\pi\epsilon R} \int_V \Delta\epsilon \exp\{i[(\mathbf{k}-\mathbf{k}_0)\cdot\mathbf{r}]\}\, d\mathbf{r}$$

where ω_0 is the circular frequency, t is the time, $\mathbf{r}$ is the radius vector from the origin of the co-ordinate system, which is taken inside the volume V, $d\mathbf{r} = dxdydz$ is the volume element, $k = k_0$ is the wave number in the medium, $\mathbf{k}_0$ and $\mathbf{k}$ are the propagation vectors of the incident and scattered waves respectively (the propagation vectors of the waves scattered from different points within the volume V are almost identical because the scattered field is calculated for a point sufficiently far from V), and γ is the angle between the electric field vector of the incident wave and the direction of scattering. The m.k.s. rationalized system of units is used.

In an ionized gas at a sufficiently high frequency

$$(2) \qquad \epsilon = \epsilon_0(1 - e^2 N/\epsilon_0 m_e \omega_0^2) \sim \epsilon_0$$

where N is the number density, m_e the mass, and e the charge of electrons. The deviation in the dielectric constant is therefore given by

$$(3) \qquad \Delta\epsilon = -(e^2/m_e\omega_0^2)\Delta N.$$

Equation (1) may then be written approximately as

$$(4) \qquad E_s = -\frac{E_0 \sin\gamma\, e^2 \exp[i(\omega_0 t - kR)]}{4\pi\epsilon_0 m_e c^2 R} \int_V \Delta N \exp\{i[(\mathbf{k}-\mathbf{k}_0)\cdot\mathbf{r}]\} d\mathbf{r}$$

where $c = \omega_0/k$ is the velocity of electromagnetic waves in free space. Equation (4) shows that the scattered field E_s is proportional to that spatial Fourier component of the electron density deviation, ΔN, whose vector wave number is $\mathbf{k}-\mathbf{k}_0$.

This spatial Fourier component itself is undetermined but the mean square of its absolute value may be calculated by considerations of statistical mechanics. Such a calculation, based on the assumed validity of the Maxwell–Boltz-

mann energy distribution, is carried out in the Appendix; it closely follows the method indicated in the Appendix of Pines and Bohm (1952), but discreet singly charged positive ions are assumed rather than a uniform positive charge density. The more general case of positive ions which carry a whole multiple of the elementary charge is treated by Kahn (1959) by slightly different methods.

Equations (76) and (78) of the present Appendix may be combined to give

$$(5)\quad \overline{\left|\int \Delta N \exp[i(\mathbf{k}-\mathbf{k}_0)\,.\,\mathbf{r}]d\mathbf{r}\right|^2} = \tfrac{1}{2}VN[1+|\mathbf{k}-\mathbf{k}_0|^2/(Ne^2/\epsilon_0 KT+|\mathbf{k}-\mathbf{k}_0|^2)]$$

where K is Boltzmann's constant and T is the absolute temperature. This equation shows that the mean square value of the Fourier component of ΔN as defined by the left side of equation (5) equals VN when $Ne^2/\epsilon_0 KT \ll |\mathbf{k}-\mathbf{k}_0|^2$. For $Ne^2/\epsilon_0 KT \gg |\mathbf{k}-\mathbf{k}_0|^2$ the mean square value of the Fourier component equals $VN/2$. This conclusion differs from that of Pines and Bohm mainly in that the Fourier component of ΔN is reduced only by a factor of 2 for $Ne^2/\epsilon_0 KT \gg |\mathbf{k}-\mathbf{k}_0|^2$ and does not become vanishingly small. The difference is due to the assumptions made in the present analysis about the discreet nature of the positive charge.

The combination of equation (5) with equation (4) leads to

$$(6)\quad \overline{|E_s|^2} = \frac{E_0^2 \sin^2\gamma\, e^4 V}{16\pi^2\epsilon_0^2 m_e^2 c^4 R^2}\frac{N}{2}\left(1+\frac{|\mathbf{k}-\mathbf{k}_0|^2}{Ne^2/\epsilon_0 KT+|\mathbf{k}-\mathbf{k}_0|^2}\right).$$

Since $\overline{|E_s|^2}/E_0^2$ is the ratio of the power density of the scattered wave to the power density of the incident wave, one may write for the scattering cross section σ, defined as the power scattered per unit solid angle, unit incident power density, and unit scattering volume

$$(7)\quad \sigma = \frac{\overline{|E_s|^2}R^2}{E_0^2 V} = \left(\frac{\mu_0 e^2 \sin\gamma}{4\pi m_e}\right)^2 \frac{N}{2}\,\frac{2|\mathbf{k}-\mathbf{k}_0|^2+Ne^2/\epsilon_0 KT}{|\mathbf{k}-\mathbf{k}_0|^2+Ne^2/\epsilon_0 KT}$$

where the relationship $c^2\epsilon_0\mu_0 = 1$ has been used. It is more convenient to write equation (7) in terms of the Debye length $l_D = (\epsilon_0 KT/Ne^2)^{\frac{1}{2}}$, the wavelength of the radio wave $\lambda = 2\pi/k$, the angle θ between the propagation vectors of the incident and the scattered waves, and the scattering coefficient $\sigma_e = (\mu_0 e^2 \sin\gamma/4\pi m_e)^2$ of a single electron. With the aid of the identity $|\mathbf{k}-\mathbf{k}_0| = 4\pi\lambda^{-1}\sin(\theta/2)$ equation (7) may then be rewritten as

$$(8)\quad \sigma = \sigma_e N\,\frac{[4\pi l_D \sin(\theta/2)]^2+\frac{1}{2}\lambda^2}{[4\pi l_D \sin(\theta/2)]^2+\lambda^2}.$$

The characteristic length l_D, which occurs in equation (8), has been introduced into the study of electrolytes by Debye and Hueckel (1923); for a short discussion of its significance in plasma physics the reader is referred to Spitzer (1956).

It should be noted that in the derivation of equation (1) for the scattered field and equation (8) for the scattering cross section it was tacitly assumed

that the irregular deviations from the mean value of the dielectric constant do not vary with time. The results remain valid to a very high degree of approximation, however, if the "apparent velocities" of the irregularities (which in the present case are of the order of the thermal velocities of the particles) are much smaller than the velocity of the radio wave. This condition is usually satisfied in practice and equation (1) is used in the present paper to calculate the fluctuations of the scattered field caused by the fluctuations of $\Delta\epsilon$.

For sufficiently small values of λ equation (8) reduces to

$$\sigma = N\sigma_e. \tag{9}$$

It is possible to show by simpler and more fundamental methods than those of the present Appendix that this value of the scattering cross section results, quite apart from any assumptions as to the velocity distribution, if the spatial probability density of an electron is constant throughout the scattering volume and if the electrons are distributed independently in space. Such a distribution of electrons will be called "random" in the present paper. The above simple result for a random distribution of scatterers has been derived by Rayleigh (1871) and in somewhat greater detail by Kahn (1959). The problem is essentially the same as the problem of shot effect in a temperature-limited diode where the probability density in time of an electron is constant and the electrons are independently distributed in time; the above result could therefore also be derived by methods used by Rice (1944).

One may then state that for sufficiently small values of the radio wavelength λ the electrons scatter as if they were randomly distributed.

For sufficiently large values of λ equation (8) reduces to $\sigma = \frac{1}{2}\sigma_e N$. Thus in this case the scattering cross section is only half of what it would be if the electrons were randomly distributed. The transition occurs approximately for $\lambda = 4\pi l_D \sin(\theta/2)$ and the corresponding scattering cross section is $\sigma = \frac{3}{4}\sigma_e N$.

3. NATURE OF THE PROCESSES DETERMINING THE FREQUENCY SPECTRUM OF THE SCATTERED POWER

In the previous section the total scattered power has been calculated but no information on its frequency distribution has been obtained. It is instructive to consider the physical processes determining the spectrum of the scattered power in a semiquantitative manner before the actual calculation of it is carried out in the next section.

In an ionized gas there is generally an irregular, fluctuating electrostatic field determined by the irregular distribution of the charge density. Such an electrostatic field tends to redistribute the charged particles by "diffusion" so that they satisfy the Maxwell–Boltzmann energy distribution. If the potential of the electrostatic field is $\delta\phi$, the field tries to redistribute the charged particles with charge $-e$ so that their number density becomes proportional to

$$\exp(e\delta\phi/KT) \cong 1+e\delta\phi/KT \tag{10}$$

if for the moment one ignores the field set up as a result of redistribution. If the corresponding irregularities in density are as large as, or larger than the original irregularities responsible for the electrostatic field, then it is likely that the effect of the electrostatic field must be taken into account.

These considerations may be expressed in a semiquantitative manner by considering a Fourier component $\delta N = \delta N_0 \cos(kx)$ of the electron density fluctuations existing at a given moment and assuming that the positive ions are uniformly distributed. The potential $\delta\phi$ of the electrostatic field caused by this "space charge" is given by

$$\epsilon_0 \partial^2 \delta\phi / \partial x^2 = e\delta N_0 \cos(kx) \tag{11}$$

or

$$\delta\phi = -e\delta N / k^2 \epsilon_0. \tag{12}$$

This potential tries to redistribute the electrons, changing their number density by

$$Ne\delta\phi / KT = -(e^2 N / k^2 \epsilon_0 KT)\delta N. \tag{13}$$

If $e^2 N / k^2 \epsilon_0 KT \gg 1$ then this change, which "diffusion" under the influence of the field tries to establish, reduces substantially the original deviation in the number density. This is the conclusion of Pines and Bohm (1952), who showed that random irregularities of larger dimensions than the Debye length tend to be smoothed out. The present arguments are of a more qualitative nature than those of Pines and Bohm, on which the Appendix of the present paper is based.

One may express this result of Pines and Bohm somewhat differently by regarding the actual electron density deviation as the sum of the spontaneous deviation which would have existed in the absence of the electrostatic field and the deviation caused by the electrostatic field, ignoring temporarily the fact that the electrostatic field is actually caused by the electron density deviations. Thus if $e^2 N / k^2 \epsilon_0 KT \gg 1$ then the fluctuations of electron density caused by the electrostatic fields almost exactly cancel the spontaneous fluctuations. These spontaneous fluctuations would be caused by the random thermal motion of the electrons in the absence of the electrostatic field.

In an actual gas the density of positive ions is not uniform. The fluctuation of ion density may also be regarded as the sum of the spontaneous deviation and the deviation caused by the electrostatic field. In view of the very much greater mass of the positive ions the rate of spontaneous fluctuations of ion density is very much slower than the rate of spontaneous fluctuations of electron density. It is therefore reasonable to assume that in an actual gas the electrostatic field has a fast and a slowly fluctuating component. The fast fluctuating component causes the almost complete cancellation of the fast spontaneous electron density fluctuations but it has only a negligible effect on the motion of the positive ions. The slowly fluctuating field affects the motion of both ions and electrons and ensures that the slow electron density fluctuations (caused by these fields) almost neutralize the slow ion

density fluctuations as the results of the Appendix show. It is further reasonable to assume that the electrons, on account of their low inertia, have ample time to assume their equilibrium distribution, indicated by equation (10) corresponding to the instantaneous value of the slowly varying component of the electrostatic field. As the instantaneous distribution of electron density is almost identical with the instantaneous distribution of ion density, the slowly varying component of the electrostatic field always assumes a configuration which, if given time, would change a hypothetical uniform ion distribution to a distribution with exactly opposite ion density deviations to those actually existing in the gas. This explains qualitatively why the electrostatic fields reduce the mean square value of the Fourier component of the ion density deviation for sufficiently small wave numbers by a factor of 2, as shown by the results of the Appendix.

If the relatively small effect of the electric field on the motion of the ions were neglected, then the calculation of the spectrum of the scattered power would be relatively simple. For $\lambda \ll 4\pi l_D \sin(\theta/2)$ the spectrum would be that appropriate to electrons executing their random thermal motion at the temperature of the gas. For $\lambda \gg 4\pi l_D \sin(\theta/2)$ the spectrum would be that appropriate to ions executing their random thermal motion corresponding to the temperature of the gas, provided that these ions are assumed to scatter radio waves as if they were electrons. This last statement is, of course, not quite correct in view of what has already been said about the effect of the electrostatic field on the motion of the ions; this effect is examined in greater detail in the next section.

4. FREQUENCY SPECTRUM OF THE SCATTERED POWER

4.1 Introduction

The following calculation of the frequency spectrum of the scattered power is carried out in two steps. It is first assumed that the scatterers execute their random thermal motion uninfluenced by fluctuating electrostatic fields. Only the two extreme cases, in which the mean free path of the particles is either very large or very small are considered. The results of this calculation are strictly valid if $\lambda \ll 4\pi l_D \sin(\theta/2)$. They are "approximately" valid for $\lambda \gg 4\pi l_D \sin(\theta/2)$ provided that the mass which determines the thermal motion of the particles is taken as the ionic mass but the mass which determines the scattering properties is taken as the electronic mass.

In the second part of the calculation this latter "approximate" result is corrected for the effect of the electrostatic field on the motion of the positive ions. The same two extreme cases are again considered.

4.2 Scattering by Charged Particles in Random Thermal Motion

If the effect of collisions is negligible then the scattering particles may be sorted into groups such that the velocities of all particles belonging to the same group are almost identical and that the particles within each group are randomly distributed in space. The power scattered by a single group is, then, in terms of equation (9) and the subsequent discussion, equal to the

product of the scattering coefficient of a single particle and the number of particles in the group. The frequency of the signal scattered by a single group differs from the frequency of the incident wave by the Doppler shift caused by the common velocity of the particles. This suggests that it is more convenient to sort the particles into groups such that the velocities of particles within the same group lead to the same Doppler shift. The shape of the frequency spectrum is then determined by the distribution of the particles into these groups and thus by the velocity distribution of the particles.

The Doppler shift in the frequency of the scattered wave is caused by that component of the particle velocity which is perpendicular to the bisector of the angle θ formed by the direction of incidence and the direction of scattering. If v is written for this component, the Doppler shift is

$$\omega-\omega_0 = (\omega_0 v/c)2\sin(\theta/2) \tag{14}$$

where ω_0 and ω are the circular frequencies of the incident and the scattered wave respectively.

The Maxwellian distribution of velocities, written in terms of a single component, shows that the number of particles with velocity components between v and $v+dv$ is proportional to

$$\exp(-mv^2/2KT)\,dv \tag{15}$$

and therefore, if the value of v from equation (14) is substituted, the number of particles which scatter with Doppler shifts between $\omega-\omega_0$ and $\omega+d\omega-\omega_0$ is seen to be proportional to $S_1(\omega)\,d\omega$ where the spectrum function $S_1(\omega)$ is given by

$$S_1(\omega) = \exp[-(\omega-\omega_0)^2/\Omega_1^2] \tag{16}$$

where Ω_1 is defined by

$$\Omega_1 = (8KT/m)^{\frac{1}{2}}(\omega_0/c)\sin(\theta/2). \tag{17}$$

The quantity $S_1(\omega)d\omega$ is also proportional to the power scattered within the frequency range extending from ω to $\omega+d\omega$ in view of the introductory remarks of this section. Therefore, if the effect of collisions is negligible, then the frequency power spectrum has the Gaussian form indicated by $S_1(\omega)$ of equation (16). The function $S_1(\omega)$ is also shown by the broken curve of Fig. 1.

Collisions have the effect of "slowing down" the motion of an individual particle by continuously changing the direction of its travel, and they may thereby reduce the spectral spreading just calculated. The fraction of particles which, in a time interval t long compared to the collision interval, suffer displacements which have components in a given direction between x and $x+dx$ is proportional to (see, for example, equation (172) of Chandrasekhar (1943))

$$\exp(-x^2/4Dt)dx \tag{18}$$

where D is the diffusion coefficient of the particle.

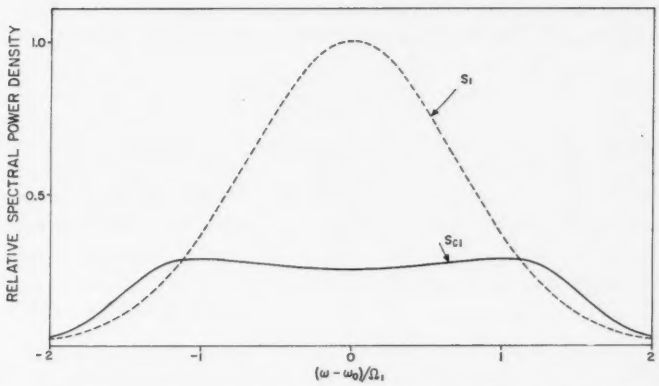

FIG. 1. The spectrum functions $S_1(\omega)$ and $S_{c1}(\omega)$ of the low collision frequency approximation. Ω_1 is given by equation (17).

In specifying the particle distribution at the beginning and end of the time interval t, one is free to assume that the particles have moved with a hypothetical velocity distribution

$$\exp(-v^2t/4D)dv \tag{19}$$

and such a velocity distribution would in the absence of collisions lead to a frequency spectrum

$$\exp[-c^2t(\omega-\omega_0)^2/16\,D\omega_0^2\sin^2(\theta/2)]. \tag{20}$$

This frequency spectrum does not actually occur, but the relationship between the particle distributions existing at the beginning and end of the time interval t can be determined correctly by applying it. The hypothetical autocorrelation function $\rho_1(\tau)$ obtained by taking the Fourier transform of the power spectrum (20) therefore gives the correct autocorrelation coefficient of the received signal for $\tau = t$. This hypothetical autocorrelation function is given by

$$\rho_1(\tau) \propto \int \exp[-c^2t(\omega-\omega_0)^2/16\,D\omega_0^2\sin^2(\theta/2)]\exp(-i\omega\tau)\,d\omega$$

or

$$\rho_1(\tau) = \exp[-i\omega_0\tau - 4D\omega_0^2\sin^2(\theta/2)\,\tau^2/c^2t]. \tag{21}$$

The value of $\rho_1(\tau)$ is applicable to the actual problem only for the one value $\tau = t$, but the calculation may be repeated for each t in turn. This then leads to the correct autocorrelation function of the physical problem

$$\rho(t) = \exp[-i\omega_0t - 4D\omega_0^2\sin^2(\theta/2)|t|/c^2]. \tag{22}$$

The Fourier transform of (22) is proportional to the frequency power spectrum of the scattered waves. It is given by

$$S^2(\omega) = [1+c^4(\omega-\omega_0)^2/16\,D^2\omega_0^4\sin^4(\theta/2)]^{-1}. \tag{23}$$

The function $S_2(\omega)$ is shown by the broken curve of Fig. 2.

The coefficient of diffusion D may be written in the form (Chandrasekhar 1943)

$$D = KT/mB \tag{24}$$

where B is the frictional coefficient in the Langevin equation for the motion of the particle, which for the present purposes may be treated as a Brownian particle. If the particles were electrons and collisions were mainly with neutral particles then B would be equal to the electron-neutral collision frequency.

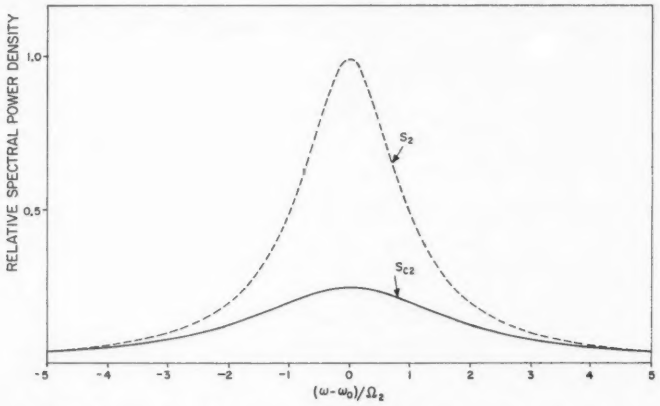

FIG. 2. The spectrum functions $S_2(\omega)$ and $S_{c2}(\omega)$ of the high collision frequency approximation. Ω_2 is given by equation (38).

The spectrum functions given by equations (16) and (23) represent two extreme cases. Some rough criterion is needed as to when collisions are sufficiently frequent to modify equation (16) and make equation (23) a better approximation. Collisions are expected to make the spectrum narrower and therefore it would be reasonable to assume that (23) is a better approximation than (16) when the power band width of the spectrum expressed by it is narrower.

Integration shows that the "power band widths" of the spectra expressed by (16) and (23) are equal for

$$\lambda = \pi^2 l_m \sin(\theta/2) \tag{25}$$

where

$$l_m = B^{-1} (8KT/\pi m)^{\frac{1}{2}} \tag{26}$$

is the mean free path of the particle.

If $\lambda \ll \pi^2 l_m \sin(\theta/2)$ one would therefore use equation (16) for the spectrum; if $\lambda \gg \pi^2 l_m \sin(\theta/2)$ equation (23) would be appropriate. As mentioned in the

introduction to the present section, the results of this subsection are strictly valid only if $\lambda \ll 4\pi l_D \sin(\theta/2)$ and in this case B, m, D, and l_m in equations (16) and (23) must be taken as the values appropriate to electrons.

If $\lambda \gg 4\pi l_D \sin(\theta/2)$ the results of the present subsection may still be regarded as a first approximation to the power spectrum of scattering provided that B, m, D, and l_m represent values appropriate to ions. Thus in the first approximation the width of the spectrum is very considerably reduced when $\lambda \gg 4\pi l_D \sin(\theta/2)$ but the shape of the spectrum is not changed very much. The more correct treatment in the next subsection shows that, if the effect of the electrostatic fields on the ion motion is taken into account, this results in a considerable change in the shape of the spectrum in addition to the reduced width when $\lambda \gg 4\pi l_D \sin(\theta/2)$.

4.3 Effect of the Electrostatic Field on the Spectrum

In this subsection the condition $\lambda \gg 4\pi l_D \sin(\theta/2)$ is assumed and the approximate results of the previous subsection are corrected for the influence of the electrostatic field, caused by the momentary charge distribution, on the motion of the ions.

The high collision frequency approximation, characterized by $\lambda \gg \pi^2 l_m \sin(\theta/2)$ with l_m appropriate to ions, is considered first. The first "approximation" to the spectrum of scattered power is then given by $S_2(\omega)$ of equations (23) and (24) with values of m and B appropriate to ions. Calculation of the correction to the spectrum function $S_2(\omega)$ for the effect of the electrostatic field on the motion of the ions follows.

It was shown in Section 2 that the amplitude of the wave scattered in a given direction is determined by the spatial Fourier component with wave number $\mathbf{k}-\mathbf{k}_0$ of the electron density deviation ΔN. The variation with time of the scattered field may therefore be determined from the variation with time of the Fourier component, which according to equation (4) is proportional to $E_s \exp(-i\omega_0 t)$. The spatial Fourier component may be written in the form of a Fourier integral in time (omitting numerical factors involving π) in the form

$$\int s(\mathbf{k}-\mathbf{k}_0,\omega') \exp(i\omega' t) d\omega'. \tag{27}$$

Since $E_s \exp(-i\omega_0 t)$ is proportional to this expression one has

$$E_s \propto \int s(\mathbf{k}-\mathbf{k}_0,\omega') \exp[i(\omega_0+\omega')t] d\omega'. \tag{28}$$

Equation (28) shows that $s(\mathbf{k}-\mathbf{k}_0,\omega')$ is proportional to the amplitude of those scattered waves whose frequency is $\omega = \omega_0+\omega'$ or whose frequency differs by $\omega' = \omega-\omega_0$ from the frequency ω_0 of the incident wave.

An alternative interpretation of $s(\mathbf{k}-\mathbf{k}_0,\omega')$ exists in terms of an elementary electron density deviation. The total electron density deviation ΔN may be written in terms of the Fourier component (27) in the form

$$\Delta N = \int \{\int s(\mathbf{k}-\mathbf{k}_0,\omega') \exp(i\omega' t) d\omega'\} \exp[-i(\mathbf{k}-\mathbf{k}_0).\mathbf{r}] d(\mathbf{k}-\mathbf{k}_0) \tag{29}$$

so that an elementary contribution δN to this integral in the vicinity of ω' and $\mathbf{k}-\mathbf{k}_0$ may be written in the form

$$\delta N = s(\mathbf{k}-\mathbf{k}_0,\omega') \exp[i(\omega' t-|\mathbf{k}-\mathbf{k}_0|x)]\delta\omega'\delta(\mathbf{k}-\mathbf{k}_0) \tag{30}$$

if the x axis is taken parallel to $\mathbf{k}-\mathbf{k}_0$.

The effect of the electrostatic field on the ion motion causes the actual ion number density deviation δN to differ from the hypothetical ion number density deviation δN_r which would have existed if the spontaneous random thermal motion of the ions had not been modified by the electrostatic field. One may regard δN as the sum of this spontaneous value δN_r and the deviation δN_t caused by the electrostatic field. This electrostatic field, the slowly varying component of Section 3, has just the correct value to keep the electron density deviation equal to the ion density deviation. Since the ion density corresponding to the deviation δN is $N+\delta N$, the electrostatic potential $\delta\phi$ required to make the electron density also equal to $N+\delta N$ satisfies a relation which follows from equation (10). This relation is

$$(N+\delta N)/N \cong 1+e\delta\phi/KT \tag{31}$$

or

$$\delta\phi = (KT/eN)\delta N. \tag{32}$$

The deviation δN_t caused by this potential $\delta\phi$ may be determined from the diffusion equation (see, for example, Chandrasekhar (1943) equation (311))

$$\partial(\delta N_t)/\partial t = (Ne/Bm) \text{ div grad } \delta\phi + (KT/mB) \text{ div grad } \delta N_t \tag{33}$$

and with the aid of equations (30) and (32) one may rewrite equation (33) in the form

$$i\omega'\delta N_t = -(KT/mB)|\mathbf{k}-\mathbf{k}_0|^2(\delta N+\delta N_t) \tag{34}$$

and thus

$$\delta N_r = \delta N-\delta N_t = \delta N(1-2iKT|\mathbf{k}-\mathbf{k}_0|^2/\omega' mB)/(1-iKT|\mathbf{k}-\mathbf{k}_0|^2/\omega' mB). \tag{35}$$

Equation (35) shows that the Fourier component of the spontaneous electron density fluctuations of wave number $\mathbf{k}-\mathbf{k}_0$ is reduced by a factor

$$[1+(KT|\mathbf{k}-\mathbf{k}_0|^2/\omega' mB)^2]^{\frac{1}{2}}[1+4(KT|\mathbf{k}-\mathbf{k}_0|^2/\omega' mB)^2]^{-\frac{1}{2}} \tag{36}$$

and thus the power density of the scattered waves in the vicinity of the frequencies $\omega_0+\omega'$ and $\omega_0-\omega'$ is reduced by a factor equal to the square of expression (36). Using equation (24) and the identity $|\mathbf{k}-\mathbf{k}_0| = 2\omega_0 c^{-1}\sin(\theta/2)$ the reduction factor may be written in the form

$$[1+\omega'^2c^4/16D^2\omega_0^4\sin^4(\theta/2)]/[4+\omega'^2c^4/16D^2\omega_0^4\sin^4(\theta/2)]. \tag{37}$$

Abbreviating

$$\Omega_2 = 4D\omega_0^2\sin^2(\theta/2)/c^2 \tag{38}$$

the spectrum described by (23) takes the form

$$S_2(\omega') = (1+\omega'^2/\Omega_2^2)^{-1} \tag{39}$$

and after multiplication by the correction factor (37) the corrected spectrum function becomes

$$S_{c2}(\omega') = (4+\omega'^2/\Omega_2^2)^{-1}. \tag{40}$$

The function $S_{c2}(\omega')$ is shown by the solid curve of Fig. 2. Integration shows that

$$\int_{-\infty}^{\infty} S_2(\omega')d\omega' = 2\int_{-\infty}^{\infty} S_{c2}(\omega')d\omega' \tag{41}$$

in agreement with the theory of Section 2. The reduction of the total scattered power by a factor of 2 is caused mainly by the reduction of the power scattered near the frequency of the incident wave, as the solid curve of Fig. 2 shows.

Equation (40) applies to the high collision frequency approximation or for $\lambda \gg \pi^2 l_m \sin(\theta/2)$, where l_m has the value given by equation (26) for positive ions.

For low collision frequencies ($\lambda \ll \pi^2 l_m \sin(\theta/2)$ with l_m appropriate to ions) the first approximation to the spectrum of the scattered power is given by equations (16) and (17) with m taken as the mass of an ion. Calculation of the correction of these equations closely follows the calculation for high collision frequencies up to equation (32). The deviation δN_f caused by the electrostatic field is not determined, however, by the diffusion equation. The appropriate equation which governs the motion of positive ions in the electrostatic field derived from the potential $\delta\phi$ is equation (249) of Chandrasekhar (1943) with the right-hand side set equal to zero

$$\partial W'/\partial t + \mathbf{v}\,\mathrm{grad}_r\, W' + \mathbf{F}.\mathrm{grad}_v\, W' = 0 \tag{42}$$

where W' is the distribution function of positive ions (over positions and velocities), $\mathrm{grad}_r\, W'$ is calculated by differentiation with respect to spatial co-ordinates, and $\mathrm{grad}_v\, W'$ is calculated by differentiation with respect to velocity components. $\mathbf{F}$ is the force per unit mass acting on the ions and in the present case it is given by

$$\mathbf{F} = -(e/m)\,\mathrm{grad}\,\delta\phi = -(KT/mN)\,\mathrm{grad}\,\delta N$$

$$F = i|\mathbf{k}-\mathbf{k}_0|(KT/mN)s(\mathbf{k}-\mathbf{k}_0,\omega')\exp[i(\omega' t-|\mathbf{k}-\mathbf{k}_0|x)]\delta\omega'\delta(\mathbf{k}-\mathbf{k}_0). \tag{43}$$

If the velocity distribution of the unperturbed gas is assumed Maxwellian, one may write

$$W' = (1+W)(m/2\pi KT)^{\frac{3}{2}}\exp(-m|\mathbf{v}|^2/2KT) \tag{44}$$

where the perturbation W is a function of the velocity. If this expression is substituted into equation (42), one obtains for the x component after linearization

$$\partial W/\partial t + v_x \partial W/\partial x - (m/KT)v_x F = 0. \tag{45}$$

Substitution of F from (43) into (45) leads to

$$W = N^{-1}\frac{|\mathbf{k}-\mathbf{k}_0|v_x \exp[i(\omega' t-|\mathbf{k}-\mathbf{k}_0|x)]}{\omega'-|\mathbf{k}-\mathbf{k}_0|v_x} s(\mathbf{k}-\mathbf{k}_0,\omega')\delta\omega'\delta(\mathbf{k}-\mathbf{k}_0) \tag{46}$$

and with the aid of (30) one may rewrite equation (46) in the form

$$W = \frac{|\mathbf{k}-\mathbf{k}_0|v_x}{\omega'-|\mathbf{k}-\mathbf{k}_0|v_x}\delta N/N. \tag{47}$$

One has to integrate the perturbation $(m/2\pi KT)^{\frac{3}{2}}W\exp(-m|\mathbf{v}|^2/2KT)$ in the distribution function W' over all velocity space to obtain the fractional perturbation $\delta N_i/N$ in the ion number density caused by the electrostatic potential $\delta\phi$. Only the integration over the x component has to be carried out in detail, the other two components merely leading to a factor $(m/2\pi KT)^{-1}$. With the aid of equation (47) one obtains for the perturbation ion density

$$\delta N_i = \delta N(m/2\pi KT)^{\frac{1}{2}}\int_{-\infty}^{\infty}\frac{|\mathbf{k}-\mathbf{k}_0|v_x}{\omega'-|\mathbf{k}-\mathbf{k}_0|v_x}\exp(-mv_x^2/2KT)dv_x. \tag{48}$$

The integrand on the right of equation (48) has an infinity at $v_x = \omega'/|\mathbf{k}-\mathbf{k}_0|$.

The evaluation of this type of integral has been first discussed in connection with plasma oscillation by Landau (1946). The results are reviewed by Berz (1956). In terms of these results the integral in equation (48) can be replaced by its principal value plus πi times the residue of the pole of the integrand (cf. equation (16*b*) of Berz). This leads to

$$\delta N_i = \delta N\Big[-1+2(\omega'/\Omega_1)\exp(-\omega'^2/\Omega_1^2)\int_0^{\omega'/\Omega_1}\exp u^2 du + i\pi^{\frac{1}{2}}(\omega'/\Omega_1)\exp(-\omega'^2/\Omega_1^2)\Big] \tag{49}$$

where Ω_1 is defined by (17) with m denoting the mass of a positive ion. Equation (49) may be rewritten with the help of the relation $\delta N = \delta N_i + \delta N_r$ in the form

$$\delta N = \delta N_r\Big[2-2(\omega'/\Omega_1)\exp(-\omega'^2/\Omega_1^2)\int_0^{\omega'/\Omega_1}\exp u^2 du - i\pi^{\frac{1}{2}}(\omega'/\Omega_1)\exp(-\omega'^2/\Omega_1^2)\Big]. \tag{50}$$

Equation (50) shows how the spontaneous fluctuations δN_r are modified by the action of electrostatic fields in the absence of collisions. Since the scattered power is proportional to the square of the electron density deviation and since the uncorrected spectrum $S_1(\omega)$ is given by equation (16) the corresponding spectrum $S_{c1}(\omega')$ is given by

$$(51)\quad S_{e1}(\omega') = \frac{\exp(-\omega'^2/\Omega_1^2)}{4\left[1-(\omega'/\Omega_1)\exp(-\omega'^2/\Omega_1^2)\int_0^{\omega'/\Omega_1}\exp u^2 du\right]^2+\pi[(\omega'/\Omega_1)\exp(-\omega'^2/\Omega_1^2)]^2}.*$$

This spectrum is shown by the solid curve of Fig. 1. Numerical integration shows that

$$(52)\qquad \int_{-\infty}^{\infty} S_1(\omega')d\omega' = 2\int_{-\infty}^{\infty} S_{e1}(\omega')d\omega'$$

in agreement with the theory of Section 2.* The reduction of the total scattered power by a factor of 2 is caused again mainly by a reduction of the power scattered near the frequency of the incident wave. The resulting spectrum function is flat-topped with slightly raised shoulders symmetrically placed about the frequency of the incident wave.

5. CONCLUSIONS

An expression for the scattering cross section σ has been obtained in the form of equation (8) in terms of the scattering coefficient σ_e of a single electron, the number density N of electrons, the wavelength λ of the incident wave, the angle θ between the propagation vectors of the incident and scattered waves, and the Debye length l_D. If $\lambda \ll 4\pi l_D \sin(\theta/2)$ then equation (8) results in the scattering cross section $\sigma = N\sigma_e$ while if $\lambda \gg 4\pi l_D \sin(\theta/2)$ equation (8) yields $\sigma = \frac{1}{2}N\sigma_e$.

In a short review of the results obtained for the frequency spectrum of the scattered power let the case of $\lambda \ll 4\pi l_D \sin(\theta/2)$ be considered first. If at the same time $\lambda \ll \pi^2 l_{me} \sin(\theta/2)$ where l_{me} is the mean free path of electrons, the spectrum has a Gaussian distribution given by equation (16) and (17) with m indicating the mass of an electron. If on the other hand $\lambda \gg \pi^2 l_{me} \sin(\theta/2)$ then the spectrum is narrower and is given by equation (23) with D taken as the diffusion coefficient of electrons.

Considering the case of $\lambda \gg 4\pi l_D \sin(\theta/2)$ one finds that the spectrum is very much narrower because its width is largely determined by the thermal motion of the ions rather than of the electrons. For $\lambda \gg \pi^2 l_{mi} \sin(\theta/2)$ the spectrum function is given approximately by equations (40) and (38) with D taken as the diffusion coefficient of ions. The shape of the spectrum function is shown by the solid curve of Fig. 2.

For $\lambda \ll \pi^2 l_{mi} \sin(\theta/2)$ the spectrum function given by equations (51) and (17), with m taken as the mass of an ion, is obtained. The shape of the spectrum function is shown by the solid curve of Fig. 1.

The effects of a uniform magnetic field on the scattering of radio waves by an ionized gas in thermal equilibrium were not considered in the present paper.

*Equation (51) has been derived independently by J. P. Dougherty and D. T. Farley at the Cavendish Laboratory, using different methods; they also establish equation (52) analytically (private communication).

It is, however, reasonable to assume that if, as in certain ionospheric applications, the gyroradius of positive ions is much greater than $\lambda/4\pi \sin(\theta/2)$ and if $\mathbf{k}-\mathbf{k}_0$ is not nearly perpendicular to the magnetic field then the results of the present paper are not seriously affected by the presence of the magnetic field. If, however, these conditions are not fulfilled, a reformulation of the theory becomes necessary.

ACKNOWLEDGMENTS

The author would like to acknowledge many helpful discussions held with Drs. R. E. Barrington, C. O. Hines, R. I. Primich, and I. Paghis. The work was performed under Project PCC No. D48-95-11-01.

REFERENCES

BERZ, F. 1956. Proc. Phys. Soc. (London) B, **69**, 939.
BOOKER, H. G. and GORDON, W. E. 1950. Proc. I.R.E. **38**, 401.
BOOKER, H. G., RATCLIFFE, J. A., and SHINN, D. H. 1950. Phil. Trans. Roy. Soc. A, **242**, 579.
BOWLES, K. L. 1958. Phys. Rev. Letters, **1**, 454.
——— 1959. Natl. Bur. Standards Rept. 6070.
CHANDRASEKHAR, D. 1943. Revs. of Modern Phys. **15**, 1.
DEBYE, P. and HUECKEL, E. 1923. Physik. Z. **24**, 185.
GORDON, W. E. 1958. Proc. I.R.E. **46**, 1824.
KAHN, F. D. 1959. Astrophys. J. **129**, 205.
LANDAU, L. 1946. J. Phys. U. S. S. R. **10**, 25.
PINES, D. and BOHM, D. 1952. Phys. Rev. **85**, 338.
LORD RAYLEIGH. 1871. Phil. Mag. Ser. **4**, 107.
RICE, S. O. 1944. Bell System Tech. J. **23**, 282.
SPITZER, L. 1956. Physics of fully ionized gases (Interscience Publishers).

APPENDIX

FOURIER ANALYSIS OF THE SPONTANEOUS DENSITY FLUCTUATIONS BASED ON THE MAXWELL–BOLTZMANN ENERGY DISTRIBUTION

The present calculation closely follows that given in Appendix I of a paper by Pines and Bohm (1952), who obtain the mean square amplitude of the spatial Fourier component of electron density fluctuations. Pines and Bohm assume a background of uniform positive charge density while the present calculation assumes discreet singly charged positive ions.

Attention should be drawn at this stage to an apparent error in the calculation of Pines and Bohm (1952). In their equation (A6) the second term inside the curly bracket on the right should be $\sum_i(\delta N_i)^2/N_0$ rather than $\sum_i(\delta N_i)^2/2N_0$ and therefore the expression on the right of the final equation (A12) should be $nk^2/[(2\pi Ne^2/KT)+k^2]$ and not $nk^2/[(4\pi Ne^2/KT)+k^2]$.

A gas containing on the average N electrons and N singly charged positive ions per unit volume is considered. An unspecified number of neutral particles may also be present. Thermal equilibrium is assumed. It is further assumed that the probability that the nth particle lies between $\mathbf{r}_n$ and $\mathbf{r}_n+d\mathbf{r}_n$ (i.e. that its three Cartesian co-ordinates lie between x_n and x_n+dx_n, y_n and y_n+dy_n, z_n and z_n+dz_n) while its momentum lies between $\mathbf{p}_n$ and $\mathbf{p}_n+d\mathbf{p}_n$ (the $\mathbf{p}$ notation is similar to the $\mathbf{r}$ notation) is

$$(53)\qquad W'(\mathbf{r}_1, \mathbf{r}_2 \ldots \mathbf{p}_1, \mathbf{p}_2 \ldots)d\mathbf{r}_1 d\mathbf{r}_2 \ldots d\mathbf{p}_1 d\mathbf{p}_2 \ldots \propto \exp(-E/KT)\, d\mathbf{r}_1 d\mathbf{r}_2 \ldots d\mathbf{p}_1 d\mathbf{p}_2 \ldots$$

where $d\mathbf{r}_1$ denotes the volume element $dx_1 dy_1 dz_1$, and E the total energy of the system, the sum of kinetic and potential energy, is given by

$$(54)\qquad E = \sum_n (p_n^2/2m_n) + \tfrac{1}{2} \sum_n \sum_{m \neq n} e_m e_n / 4\pi\epsilon_0 r_{mn}.$$

Here e_m and e_n are the charges of the mth and nth charged particles, r_{mn} is the distance between them, m_n is the mass of the nth particle, and ϵ_0 the dielectric constant of free space. If the integration over momentum space is carried out, the probability of a given spatial distribution of the charged particles is obtained in the form

$$(55)\qquad W'(\mathbf{r}_1, \mathbf{r}_2 \ldots)d\mathbf{r}_1 d\mathbf{r}_2 \ldots \propto \exp(-\tfrac{1}{2} \sum_n \sum_{m \neq n} e_m e_n / 4\pi\epsilon_0 r_{mn} KT) d\mathbf{r}_1 d\mathbf{r}_2 \ldots.$$

Let the available space be divided into cells of equal volume w such that each cell contains a large number of charged particles and yet each cell is small enough so that no important physical property changes within a cell. Let the ith cell contain n_{i+} singly charged positive ions and n_{i-} electrons. Then the probability $W(n_{1+}, n_{1-}, n_{2+}, n_{2-} \ldots n_{i+}, n_{i-} \ldots)$ that the first cell contains n_{1+} ions and n_{1-} electrons, the second cell contains n_{2+} ions and n_{2-} electrons etc. is the product of the probability of any specific combination of the individual particles into the cells, which leads to the required occupation numbers and of the total number of different combinations leading to these same occupation numbers.

Using these occupation numbers the probability density of a specific combination is, according to equation (55), proportional to

$$(56)\qquad \exp(-\tfrac{1}{2} \sum_n \sum_{m \neq n} e_m e_n / 4\pi\epsilon_0 r_{mn} KT) = \exp\left[-\frac{e^2}{8\pi\epsilon_0 KT} \sum_j \sum_{i \neq j} \frac{(n_{i+} - n_{i-})(n_{j+} - n_{j-})}{|\mathbf{r}_i - \mathbf{r}_j|} \right]$$

where $\mathbf{r}_i$ and $\mathbf{r}_j$ are the radius vectors to the centers of the ith and jth cells and where the contributions of pairs of particles situated in the same cell are omitted from the right. This latter step is justified by the fact that the final results are independent of the size of the cells.

The total number of different combinations leading to the required occupation numbers is $(n!/n_{1+}!n_{2+}! \ldots)(n!/n_{1-}!n_{2-}! \ldots)$ where $n = \sum_i n_{i+} = \sum_i n_{i-}$ is the total number of electrons (or ions). Setting $n_{i+} = n_0 + \delta n_{i+}$ and $n_{i-} = n_0 + \delta n_{i-}$, where n_0 is the mean number of electrons in a cell, one obtains for the required probability

$$(57)\qquad W(n_{1+}, n_{1-}, n_{2+} \ldots) = \frac{n!}{n_{1+}!n_{2+}! \ldots} \frac{n!}{n_{1-}!n_{2-}! \ldots} \exp\left[-\frac{e^2}{8\pi\epsilon_0 KT} \sum_{i \neq j} \frac{(\delta n_{i+} - \delta_{n\,i-})(\delta n_{j+} - \delta n_{j-})}{|\mathbf{r}_i - \mathbf{r}_j|} \right].$$

From Stirling's formula

$$n!/n_{1+}!\,n_{2+}!\ldots \cong \exp\{n\,ln\,n-\sum_i[(n_0+\delta n_{i+})ln(n_0+\delta n_{i+})]\}.$$

If $\delta n_{i+} \ll n_0$ then one may write $ln(n_0+\delta n_{i+}) \cong ln\,n_0+\delta n_{i+}/n_0$ and thus

$$n!/n_{1+}!\,n_{2+}!\ldots \cong \exp\{n\,ln\,n-\sum_i[n_0 ln\,n_0+(\delta n_{i+})^2/n_0]\} \tag{58}$$

since $\sum_i \delta n_{i+} = 0$. Substitution of (58) into (57) results in

$$W(n_{1+}, n_{1-}, n_{2+}\ldots) \propto \exp\left\{-\frac{e^2}{8\pi\epsilon_0 KT}\sum_j \sum_{i\neq j}\frac{(\delta n_{i+}-\delta n_{i-})(\delta n_{j+}-\delta n_{j-})}{|\mathbf{r}_i-\mathbf{r}_j|} - \sum_i [(\delta n_{i+})^2+(\delta n_{i-})^2]/n_0\right\}. \tag{59}$$

Since the n_{i+}, n_{i-} are very large numbers, one may regard δn_{i+} and δn_{i-} as continuous variables and one may then consider equation (59) as the probability density in n_{i+}, n_{1-}, n_{2+}, ... space which must be multiplied by the volume element $dn_{1+}\,dn_{1-}\,dn_{2+}\ldots$ to obtain the probability. Each side of equation (59) can then also be interpreted as the probability that the number of particles in the first cell is between $n_{1+}-\frac{1}{2}$ and $n_{1+}+\frac{1}{2}$ etc., since this leads to a volume element $dn_{1+}\,dn_{1-}\,dn_{2+}\ldots$ of unity.

It is convenient to introduce new variables $\delta n_{id} = \delta n_{i+}-\delta n_{i-}$, $\delta n_{is} = \delta n_{i+}+\delta n_{i-}$. The Jacobian of this transformation is a constant so that the probability density in n_{id}, n_{is} space is given by

$$W \propto \exp\left\{-\frac{e^2}{8\pi\epsilon_0 KT}\sum_j \sum_{i\neq j}\frac{\delta n_{id}\delta n_{jd}}{|\mathbf{r}_i-\mathbf{r}_j|}-\tfrac{1}{2}\sum_i [(\delta n_{id})^2+(\delta n_{is})^2]/n_0\right\}. \tag{60}$$

Another transformation is introduced by expanding δn_{id} and δn_{is} into Fourier series with periodic boundary conditions, assuming the total volume to have the shape of a cube of volume V.

The equations of transformation are then

$$\delta n_{id} = \sum_{\mathbf{k}} w a_{\mathbf{k}d}\exp(i\mathbf{k}.\mathbf{r}_i), \qquad \delta n_{is} = \sum_{\mathbf{k}} w a_{\mathbf{k}s}\exp(i\mathbf{k}.\mathbf{r}_i) \tag{61}$$

since δn_{id} and δn_{is} are by definition only determined at points spaced $w^{\frac{1}{3}}$ apart in a cubic lattice. If the components of $\mathbf{k}$ are taken as multiples of $2\pi V^{-\frac{1}{3}}$ and if the highest value of each component of $\mathbf{k}$ is taken as $2\pi w^{-\frac{1}{3}}$ in the summations of equation (61) then there are just enough equations to determine the coefficients $a_{\mathbf{k}d}$ and $a_{\mathbf{k}s}$ unambiguously.

Since $a_{\mathbf{k}d}$ and $a_{\mathbf{k}s}$ are complex, it is convenient to write

$$a_{\mathbf{k}d} = A_{\mathbf{k}d}\exp(i\alpha_{\mathbf{k}d}), \qquad a_{\mathbf{k}s} = A_{\mathbf{k}s}\exp(i\alpha_{\mathbf{k}s}) \tag{62}$$

and then (61) and (62) may be rewritten as

$$\delta n_{id} = \sum_{\mathbf{k}}[wA_{\mathbf{k}d}\cos\alpha_{\mathbf{k}d}\cos(\mathbf{k}.\mathbf{r}_i)-wA_{\mathbf{k}d}\sin\alpha_{\mathbf{k}d}\sin(\mathbf{k}.\mathbf{r}_i)] \tag{63}$$

or

$$\delta n_{id} = \sum_{\mathbf{k}} w[c_{\mathbf{k}d}\cos(\mathbf{k}.\mathbf{r}_i)-s_{\mathbf{k}d}\sin(\mathbf{k}.\mathbf{r}_i)]$$

where

(64) $$c_{kd} = A_{kd} \cos \alpha_{kd} \qquad s_{kd} = A_{kd} \sin \alpha_{kd}$$

and there are corresponding equations with the subscript s instead of d. It is convenient to regard the transformation from δn_{id}, δn_{is} space to A_{kd}, α_{kd}, A_{ks}, α_{ks} space indicated by (61) and (62) as the sum of the two transformations (63) and (64). The Jacobian of (63) from δn_{id}, δn_{is} space to c_{kd}, s_{kd}, c_{ks}, s_{ks} space is clearly a constant and thus the volume element $\Pi_i d(\delta n_{id}) d(\delta n_{is})$ is proportional to the volume element $\Pi_k \, dc_{kd} \, ds_{kd} \, dc_{ks} \, ds_{ks}$. The further transformation (64) can be split up into individual transformations which have the nature of transformations from two-dimensional cartesian to polar co-ordinates so that $dc_{kd} \, ds_{kd} = A_{kd} \, dA_{kd} \, d\alpha_{kd}$. The volume element in A_{kd}, α_{kd}, A_{ks}, α_{ks} space is then proportional to

(65) $$\Pi_k A_{kd} A_{ks} dA_{kd} dA_{ks} d\alpha_{kd} d\alpha_{ks}.$$

It remains to rewrite equation (60) in terms of the A_{kd}, α_{kd}, A_{ks}, α_{ks} co-ordinates. It is convenient to regard the δn_{id}, δn_{is} for this purpose as continuous functions of position defined by equation (61) and rewrite equation (60) substituting integrals for the sums.

(66) $$W \propto \exp\left\{ - \frac{e^2}{8\pi\epsilon_0 KTw^2} \int \frac{\delta n_{id} \delta n_{jd}}{|\mathbf{r}_i - \mathbf{r}_j|} d\mathbf{r}_i d\mathbf{r}_j - \frac{1}{2n_0 w} \int [(\delta n_{id})^2 + (\delta n_{is})^2] d\mathbf{r}_i \right\}$$

The co-ordinate transformation relations (61) may be written as integrals in $\mathbf{k}$ space with a_{kd} and a_{ks} constant within an elementary "volume" $(2\pi)^3/V$ in $\mathbf{k}$ space. If the volume is very small, the limits of integration may be taken as infinity and the first of equations (61) becomes the Fourier transform relation

(67) $$\delta n_{id} = Vw(2\pi)^{-3} \int a_{kd} \exp(i\mathbf{k} \cdot \mathbf{r}_i) d\mathbf{k} = (2\pi)^{-\frac{3}{2}} \int (2\pi)^{-\frac{3}{2}} a_{kd} Vw \exp(i\mathbf{k} \cdot \mathbf{r}_i) d\mathbf{k}$$

and a similar equation applies to δn_{is}. Equation (67) may be modified using the convolution theorem of Fourier transforms, in the form given by equation (10) or (11) of Booker, Ratcliffe, and Shinn (1950), to obtain

(68) $$\int_{\mathbf{r}_i - \mathbf{r}_j = \text{const}} \delta n_{id} \delta n_{jd} d\mathbf{r}_i = \int |(2\pi)^{-\frac{3}{2}} a_{kd} Vw|^2 \exp[i\mathbf{k} \cdot (\mathbf{r}_i - \mathbf{r}_j)] \, d\mathbf{k}$$

where $\mathbf{r}_i - \mathbf{r}_j$ is kept constant in the integrations indicated on the left and the right. A similar equation applies to the δn_{is}. Setting $\mathbf{r}_i - \mathbf{r}_j = 0$ in (68) results in

(69) $$\int (\delta n_{id})^2 d\mathbf{r}_i = (2\pi)^{-3} V^2 w^2 \int |a_{kd}|^2 d\mathbf{k} = w^2 V \sum_{\mathbf{k}} |a_{kd}|^2.$$

Similarly the first integral in the curly bracket in (66) may be modified with the aid of (68) and using the new set of space variables $\mathbf{r}_j$ and $\mathbf{u}_i = \mathbf{r}_i - \mathbf{r}_j$ instead of the old set $\mathbf{r}_j$ and $\mathbf{r}_i$

(70) $$\int \frac{\delta n_{id} \delta n_{jd}}{|\mathbf{r}_i - \mathbf{r}_j|} d\mathbf{r}_i d\mathbf{r}_j = \int (2\pi)^{-3} w^2 V^2 |a_{kd}|^2 \left[\int |\mathbf{u}_i|^{-1} \exp(i\mathbf{k} \cdot \mathbf{u}_i) d\mathbf{u}_i \right] d\mathbf{k}.$$

The inside integral in (70) is best evaluated by changing to spherical polar co-ordinates R, θ, ϕ with $\theta = 0$ corresponding to the direction of $\mathbf{k}$ and with $R = k|\mathbf{u}_i|$ so that

$$\int |\mathbf{u}_i|^{-1} \exp(i\mathbf{k} \cdot \mathbf{u}_i) d\mathbf{u}_i = k^{-2} \int R^{-1} \exp(iR\cos\theta) R^2 \sin\theta dR d\theta d\phi$$

$$= 2\pi k^{-2} \int_0^{\infty} RdR \int_{\cos\theta=-1}^{\cos\theta=1} \exp(iR\cos\theta) d(\cos\theta) = 4\pi k^{-2} \int_0^{\infty} \sin R dR.$$

This integral does not converge if the limit is taken as infinity. Taking the limit temporarily as kL where L is a very large value of $|\mathbf{r}_i - \mathbf{r}_j| = |\mathbf{u}_i|$ one obtains

$$4\pi k^{-2} \int_0^{kL} \sin R dR = 4\pi k^{-2}(1 - \cos kL)$$

and thus (70) may be rewritten in the form

$$(71) \qquad \int \frac{\delta n_{i\mathbf{d}} \delta n_{j\mathbf{d}}}{|\mathbf{r}_i - \mathbf{r}_j|} d\mathbf{r}_i d\mathbf{r}_j = \int (2\pi)^{-3} w^2 V^2 (|a_{\mathbf{kd}}|^2/k^2) 4\pi (1 - \cos kL) d\mathbf{k}.$$

The value of the integral on the right of (71) does not change by omitting the term $\cos kL$ because the integral $\int (|a_{\mathbf{kd}}|^2/k^2) \cos kL d\mathbf{k}$ vanishes if L tends to infinity. Equation (66) may then be rewritten with the aid of (69) and (71) as

$$(72) \qquad W \propto \exp\{-V\textstyle\sum_{\mathbf{k}}[(e^2/2\epsilon_0 k^2 KT)|a_{\mathbf{kd}}|^2 + (w/2n_0)(|a_{\mathbf{kd}}|^2 + |a_{\mathbf{ks}}|^2)]\}.$$

Using equation (65) and (72) one can calculate the average value of $|a_{\mathbf{kd}}|^2 = A_{\mathbf{kd}}{}^2$ and $|a_{\mathbf{ks}}|^2 = A_{\mathbf{ks}}{}^2$

$$\overline{A_{\mathbf{kd}}^2} = \frac{\int A_{\mathbf{kd}}^2 W \Pi_{\mathbf{k}} A_{\mathbf{kd}} A_{\mathbf{ks}} dA_{\mathbf{kd}} dA_{\mathbf{ks}} d\alpha_{\mathbf{kd}} d\alpha_{\mathbf{ks}}}{\int W \Pi_{\mathbf{k}} A_{\mathbf{kd}} A_{\mathbf{ks}} dA_{\mathbf{kd}} dA_{\mathbf{ks}} d\alpha_{\mathbf{kd}} d\alpha_{\mathbf{ks}}} = \frac{\int A_{\mathbf{kd}}^3 \exp(-BA_{\mathbf{kd}}^2) dA_{\mathbf{kd}}}{\int A_{\mathbf{kd}} \exp(-BA_{\mathbf{kd}}^2) dA_{\mathbf{kd}}} = B^{-1}$$

where $B = V[e^2/2\epsilon_0 k^2 KT + (2N)^{-1}]$ and thus

$$(73) \qquad \overline{A_{\mathbf{kd}}^2} = \frac{2Nk^2 V^{-1}}{Ne^2/\epsilon_0 KT + k^2}$$

and similarly

$$(74) \qquad \overline{A_{\mathbf{ks}}^2} = 2N/V.$$

If one defines in analogy to (61)

$$(75) \qquad \delta n_{i+} = \textstyle\sum_{\mathbf{k}} w a_{\mathbf{k}+} \exp(i\mathbf{k} \cdot \mathbf{r}_i), \qquad \delta n_{i-} = \sum_{\mathbf{k}} w a_{\mathbf{k}-} \exp(i\mathbf{k} \cdot \mathbf{r}_i)$$

one may write

$$\overline{|a_{\mathbf{ks}}|^2} = \overline{|a_{\mathbf{k}+} + a_{\mathbf{k}-}|^2} = \overline{|a_{\mathbf{k}+}|^2} + \overline{|a_{\mathbf{k}-}|^2} + 2\overline{|a_{\mathbf{k}+}||a_{\mathbf{k}-}| \cos(\alpha_{\mathbf{k}+} - \alpha_{\mathbf{k}-})}$$

$$\overline{|a_{\mathbf{kd}}|^2} = \overline{|a_{\mathbf{k}+} - a_{\mathbf{k}-}|^2} = \overline{|a_{\mathbf{k}+}|^2} + \overline{|a_{\mathbf{k}-}|^2} - 2\overline{|a_{\mathbf{k}+}||a_{\mathbf{k}-}| \cos(\alpha_{\mathbf{k}+} - \alpha_{\mathbf{k}-})}$$

In view of the symmetry of the distribution (55) $\overline{|a_{\mathbf{k}+}|^2} = \overline{|a_{\mathbf{k}-}|^2}$ and thus

$$(76) \qquad \overline{|a_{k-}|^2} = \tfrac{1}{4}(\overline{|a_{\mathbf{ks}}|^2} + \overline{|a_{\mathbf{kd}}|^2}) = (N/2V)[1 + k^2/(Ne^2/\epsilon_0 KT + k^2)].$$

It should be recalled at this point that $a_{\mathbf{k}-}$ is defined by an equation analogous to (67)

$$\delta n_{i-} = (2\pi)^{-\frac{3}{2}} \int (2\pi)^{-\frac{3}{2}} a_{\mathbf{k}-} V w \exp(i\mathbf{k} \cdot \mathbf{r}_i) d\mathbf{k}. \tag{77}$$

Writing $\Delta N = \delta n_{i-}/w$ for the electron density deviation the inverse form of (77) may be written as

$$a_{\mathbf{k}-} = V^{-1} \int \Delta N \exp(i\mathbf{k} \cdot \mathbf{r}) d\mathbf{r}. \tag{78}$$

Equation (76) shows that if the volume V is taken as unity then for sufficiently large values of k the mean square amplitude of the Fourier component $a_{\mathbf{k}-}$ of the electron (and ion) density fluctuations is equal to the electron density N. This value would exist in a random distribution of electrons. If on the other hand $k \ll (Ne^2/\epsilon_0 KT)^{\frac{1}{2}}$ then the mean square amplitude of the Fourier components is reduced to $N/2$.

Equation (73) shows that if the volume V is taken as unity, the mean square amplitude of the Fourier component of the difference between the electron density and the ion density is $2N$ for sufficiently large values of k. This value of the Fourier component is again appropriate to a random distribution and is in general reduced in the ratio $k^2/(k^2+Ne^2/\epsilon_0 KT)$. Thus for the values of k for which $k \ll l_D^{-1}$, where $l_D = (\epsilon_0 KT/Ne^2)^{\frac{1}{2}}$ is the Debye length, the Fourier component of the electron density distribution is almost equal to the Fourier component of the ion density distribution and the mean square value of both Fourier components is reduced by a factor of 2.

NOTES

THE ELECTRICAL RESISTANCE MAXIMUM IN DILUTE MAGNESIUM ALLOYS

G. GAUDET, F. T. HEDGCOCK, G. LAMARCHE, AND E. W. WALLINGFORD

In a recent publication by Hedgcock *et al.* (1960) some low temperature electrical resistivity measurements were reported on dilute magnesium and aluminum alloys. It is the purpose of the present note to report the occurrence of a resistance maximum discovered in magnesium–manganese alloys of higher manganese content than the alloys described in the earlier publication.

All the magnesium–manganese resistance specimens were cut from an ingot having a nominal manganese content of 1 at.%. Resistance samples obtained from the ingot were quenched from various temperatures and the resistance ratio $R_{4.2}/R_{273}$ measured for each sample. Table I contains values of the resistance ratio and an estimate of the manganese content in solid solution. The nominal concentration of manganese given in Table I was deduced from the phase diagram of the system (see Metals Handbook (1948)) and indicates that the resistance ratio increases with increasing manganese concentration as would be expected if solid solutions were formed. In order to keep as much manganese as possible in solution, the resistance specimens received no strain-relieving anneal after being quenched and before being measured.

TABLE I

$R_{4.2}/R_{273}$	Estimated atomic percentage manganese	T_{max}(°K) ±0.2	T_{min}(°K) ±1	$\frac{R_{T_{max}}-R_{T_{min}}}{R_{T_{min}}}\times 10^2$
0.152	0.16	1.2	21.3	17.8
0.212	0.22	1.9	22.6	15.0
0.328	0.35	3.3	25.4	10.0
0.371	0.40	4.0	27.0	8.8
0.498	0.56	6.3	31.0	5.8
0.527	0.60	6.7	33.0	5.2

Figure 1 shows some typical temperature resistance curves in the region of the resistance maximum. All the maxima were preceded by a pronounced minimum in the electrical resistance. Table I gives the temperature of occurrence for both the resistance maximum and minimum as well as a normalized value of the "depth" of the resistance minimum $(R_{T_{max}}-R_{T_{min}})/R_{T_{min}}$. It can be seen that the position of the resistance minimum moves to higher temperatures as the concentration of manganese is increased and that the normalized depth of the minimum decreases with increasing impurity content. It can also be seen in Table I that the temperature of the resistance maximum, T_{max}, increases as the impurity content is increased.

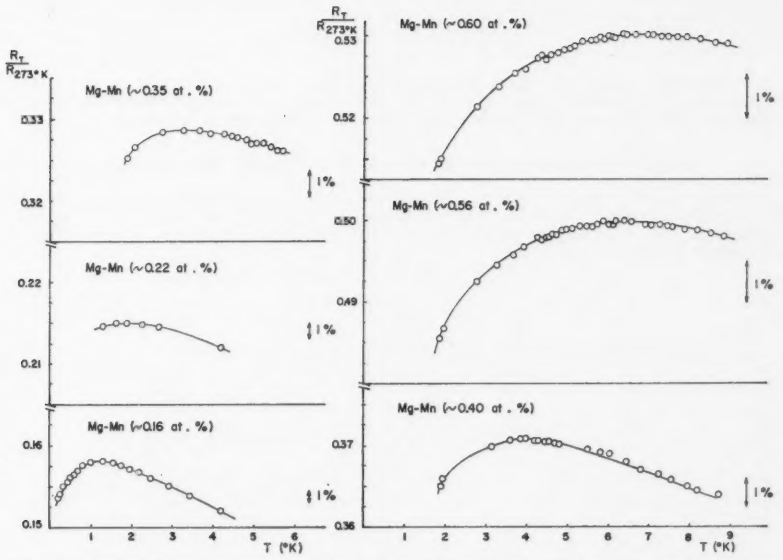

FIG. 1. Temperature dependence of the relative resistance of a number of magnesium alloys described in Table I.

The anomalous resistance behavior of the sample with a nominal manganese content of 0.16 at.% shows no evidence of levelling off even down to 0.2° K. Preliminary measurements indicate a negative magnetoresistance for these alloys in the region of the resistance maximum. Further details of the electron transport and magnetic properties of these alloys will be given in later and more detailed publications.

The fact that manganese is known to induce a resistance maximum, in the monovalent metals gold, silver, and copper (see, for example, Korringa and Gerritsen (1953)) and in the divalent metal magnesium* adds strength to the argument that only the specific nature of the impurity needs to be considered in discussing low temperature resistive anomalies.

The authors would like to thank the Dow Chemical Metallurgical Laboratories for supplying the magnesium alloys and the National Research Council of Canada for the support of this research.

HEDGCOCK, F. T., MUIR, W. B., and WALLINGFORD, E. 1960. Can. J. Phys. **38**, 376.
KORRINGA, J. and GERRITSEN, A. N. 1953. Physica, **19**, 457.
METALS HANDBOOK. 1948. (The American Society for Metals, Cleveland, Ohio).
MUTO, Y., TAWARO, Y., SHIBUYA, Y., and FUKUROI, T. 1959. J. Phys. Soc. Japan, **14**, 380.

RECEIVED MAY 3, 1960.
DEPARTMENT OF PHYSICS,
UNIVERSITY OF OTTAWA,
OTTAWA, CANADA.

*Magnetoresistance measurements made by Muto *et al.* (1959) have indicated the probable occurrence of a resistance maximum in the divalent metal zinc.

LETTERS TO THE EDITOR

Under this heading brief reports of important discoveries in physics may be published. These reports should not exceed 600 words and, for any issue, should be submitted not later than six weeks previous to the first day of the month of issue. No proof will be sent to the authors.

Frequency Measurement of Standard Frequency Transmissions[1,2]

Measurements are made at Ottawa, Canada, using N.R.C. caesium-beam frequency resonator as reference standard (with an assumed frequency of 9 192 631 770 c.p.s.). Frequency deviations from nominal are quoted in parts per 10^{10}. A negative sign indicates that the frequency is below normal.

Date, May 1960	MSF, 60 kc/s	GBR, 16 kc/s		WWVB 60 kc/s
		6-hour average*	24-hour average	
1	−140	−142	−139	N.M.
2	−149	−140	−137	−69
3	−148	−147	N.M.	−75
4	N.M.	N.M.	N.M.	−72
5	−143	−145	−143	−69
6	−140	−146	−144	−69
7	−147	−144	−144	N.M.
8	−124	−140	−144	N.M.
9	−146	−143	−145	−70
10	−134	−140	−144	−28
11	−142	−141	−142	−40
12	−149	−141	−142	−66
13	−138	−144	−141	−30
14	−141	−142	−142	N.M.
15	−138	−141	−142	N.M.
16	−142	−144	−144	−66
17	−143	−144	−142	−64
18	−141	−140	−142	−65
19	−137	−143	−139	−66
20	−155	−141	−141	−66
21	−140	−143	−141	N.M.
22	−139	−141	−141	N.M.
23	−140	−141	−141	−66
24	−131	−142	−141	−64
25	−134	−137	−139	−65
26	−146	−133	−132	−64
27	−141	−136	−134	−66
28	N.M.	−145	N.M.	N.M.
29	N.M.	N.M.	N.M.	N.M.
30	−138	N.M.	N.M.	N.M.
31	−138	−142	−144	− 3
Midmonthly mean	−141	−142	−141	
Midmonthly mean of WWV	−137			

NOTE: N.M. no measurement.
*Time of observations: 01.00 to 04.00 U.T.; 10.00 to 13.00 U.T.

RECEIVED JUNE 17, 1960.
DIVISION OF APPLIED PHYSICS,
NATIONAL RESEARCH COUNCIL,
OTTAWA, CANADA.

S. N. KALRA

[1]Issued as N.R.C. No. 5746.
[2]Cf. Kalra, S. N. 1959. Can. J. Phys. **37**, 1328.

THE PHYSICAL SOCIETY

MEMBERSHIP of the Society is open to all who are interested in Physics.

FELLOWS pay an Entrance Fee of £1 1*s*. ($3.15) and an Annual Subscription of £2 2*s*. ($6.00).

STUDENTS: A candidate for Studentship must be between the ages of 18 and 26, and pays an Annual Subscription of 5*s*. ($0.75).

MEETINGS: Fellows and Students may attend all Meetings of the Society including the annual Exhibition of Scientific Instruments and Apparatus.

PUBLICATIONS include the *Proceedings of the Physical Society*, published monthly, £12 12*s*. ($36.00) per annum, and *Reports on Progress in Physics*, published annually. Volume XXII, 1959, is now available (price £3 3*s*. ($9.45)). Members are entitled to receive any of the Publications at a reduced rate.

Further information can be obtained from:

THE PHYSICAL SOCIETY
1, LOWTHER GARDENS, PRINCE CONSORT ROAD
LONDON, S.W.7, ENGLAND

NOTES TO CONTRIBUTORS

Canadian Journal of Physics

MANUSCRIPTS

General.—Manuscripts, in English or French, should be typewritten, double spaced, on paper 8½×11 in. **The original and one copy are to be submitted.** Tables and captions for the figures should be placed at the end of the manuscript. Every sheet of the manuscript should be numbered. Style, arrangement, spelling, and abbreviations should conform to the usage of recent numbers of this journal. Greek letters or unusual signs should be written plainly or explained by marginal notes. Characters to be set in boldface type should be indicated by a wavy line below each character. Superscripts and subscripts must be legible and carefully placed. Manuscripts and illustrations should be carefully checked before they are submitted. Authors will be charged for unnecessary deviations from the usual format and for changes made in the proof that are considered excessive or unnecessary.

Abstract.—An abstract of not more than about 200 words, indicating the scope of the work and the principal findings, is required, except in Notes.

References.—References should be listed **alphabetically by authors' names,** unnumbered, and typed after the text. The form of the citations should be that used in current issues of this journal; in references to papers in periodicals, titles should not be given and only initial page numbers are required. The names of periodicals should be abbreviated in the form given in the most recent *List of Periodicals Abstracted by Chemical Abstracts.* All citations should be checked with the original articles and each one referred to in the text by the authors' names and the year.

Tables.—Tables should be numbered in roman numerals and each table referred to in the text. Titles should always be given but should be brief; column headings should be brief and descriptive matter in the tables confined to a minimum. Vertical rules should not be used. Numerous small tables should be avoided.

ILLUSTRATIONS

General.—All figures (including each figure of the plates) should be numbered consecutively from 1 up, in arabic numerals, and each figure referred to in the text. The author's name, title of the paper, and figure number should be written in the lower left corner of the sheets on which the illustrations appear. Captions should not be written on the illustrations.

Line drawings.—Drawings should be carefully made with India ink on white drawing paper, blue tracing linen, or co-ordinate paper ruled in blue only; any co-ordinate lines that are to appear in the reproduction should be ruled in black ink. Paper ruled in green, yellow, or red should not be used. All lines must be of sufficient thickness to reproduce well. Decimal points, periods, and stippled dots must be solid black circles large enough to be reduced if necessary. Letters and numerals should be neatly made, preferably with a stencil **(do NOT use typewriting)** and be of such size that the smallest lettering will be not less than 1 mm high when the figure is reduced to a suitable size. Many drawings are made too large; originals should not be more than 2 or 3 times the size of the desired reproduction. Whenever possible two or more drawings should be grouped to reduce the number of cuts required. In such groups of drawings, or in large drawings, full use of the space available should be made; the ratio of height to width should conform to that of a journal page (4⅞×7½ in.), but allowance must be made for the captions. **The original drawings and one set of clear copies (e.g. small photographs) are to be submitted.**

Photographs.—Prints should be made on glossy paper, with strong contrasts. They should be trimmed so that essential features only are shown and mounted carefully, with rubber cement, on white cardboard, with no space between those arranged in groups. In mounting, full use of the space available should be made. **Photographs are to be submitted in duplicate;** if they are to be reproduced in groups one set should be mounted, the duplicate set unmounted.

REPRINTS

A total of 100 reprints of each paper, without covers, are supplied free. Additional reprints, with or without covers, may be purchased at the time of publication.

Charges for reprints are based on the number of printed pages, which may be calculated approximately by multiplying by 0.6 the number of manuscript pages (double-spaced typewritten sheets, 8½×11 in.) and including the space occupied by illustrations. Prices and instructions for ordering reprints are sent out with the galley proof.

Contents

Peter Rastall—An approach to a theory of gravitation - - - - - - - 975

D. S. Smith—A method of precise fringe pointing - - - - - - - - 983

J. L. Wolfson and F. Terentiuk—Concentration of particulate air-borne fission products at ground level in Canada during I.G.Y. - - - - - - 991

J. Katzman and D. Venkatesan—A world-wide study of the daily variation of the nucleonic component of cosmic rays - - - - - - - - - 1011

R. J. Berry—The reproducibility of the sulphur point - - - - - - - 1027

W. B. Pearson—The thermoelectric power of annealed and cold-worked silver and gold at low temperatures - - - - - - - - - - - - - - 1048

Thomas A. Farley—Half-period of Th^{232} - - - - - - - - - - - - 1059

J. D. King, R. N. H. Haslam, and W. J. McDonald—The gamma-neutron cross section for F^{19} - - - - - - - - - - - - - - - - - 1069

T. S. Plaskett and W. C. Winegard—Cell to dendrite transition in tin base alloys - 1077

J. T. Weaver and R. Skinner—A theory of ionospheric currents associated with aurorae. I - - - - - - - - - - - - - - - - - - - 1089

J. T. Weaver and R. Skinner—A theory of ionospheric currents associated with aurorae. II - - - - - - - - - - - - - - - - - - 1104

J. A. Fejer—Scattering of radio waves by an ionized gas in thermal equilibrium - 1114

Notes:

G. Gaudet, F. T. Hedgcock, G. Lamarche, and E. W. Wallingford—The electrical resistance maximum in dilute magnesium alloys - - - 1134

Letters to the Editor:

S. N. Kalra—Frequency measurement of standard frequency transmissions 1136

Printed in Canada *by* University of Toronto Press